Journal of Materials Engineering and Performance®

Impact behaviour of A356 foundry alloys in the presence of trace elements Ni and V

Journal:	*Journal of Materials Engineering and Performance*
Manuscript ID:	JMEP-14-03-6023
Manuscript Type:	Technical Paper
Date Submitted by the Author:	04-Mar-2014
Complete List of Authors:	Casari, D.; University of Ferrara, Engineering Department Ludwig, T.; Hydro Aluminium AS, Arnberg, L.; Norwegian University of Science and Technology, Department of Materials Science and Engineering Merlin, M.; University of Ferrara, Engineering Department Garagnani, G.L.; University of Ferrara, Engineering Department
Keywords:	Aluminum, Casting, Mechanical Testing, Metallography

Impact behaviour of A356 foundry alloys in the presence of trace elements Ni and V

Daniele Casari[a,*], Thomas H. Ludwig[b], Lars Arnberg[c], Mattia Merlin[a], Gian Luca Garagnani[a]

[a] Engineering Department, University of Ferrara, Via Saragat 1, I-44122 Ferrara, Italy
[b] Hydro Aluminium AS, Verksvegen 1, N-6882 Øvre Årdal, Norway
[c] Department of Materials Science and Engineering, Norwegian University of Science and Engineering, Alfred Getz vei 2, Trondheim N-7491, Norway

ABSTRACT

In the present work, the impact behaviour of unmodified A356 alloys with the addition of Ni or V in as-cast and T6 heat treated conditions was assessed by investigating notched specimens obtained from sand and permanent mould casting. Low total absorbed energy average values (Wt < 2 J) were measured for the investigated range of alloys. SEM investigations of fracture profiles and surfaces indicated a Si-driven crack propagation with a predominant transgranular fracture mode. Occasionally, intergranular contributions to fracture were detected in the permanent mould cast alloys, most likely because of the locally finer microstructure. Complex and interconnected mechanisms related to the chemical composition (V solid solution strengthening within α-Al matrix), solidification conditions (SDAS and eutectic Si particle size) and heat treatment (precipitation of coherent Mg_2Si particles) were found to interact during the fracture process, thus governing the impact properties of the examined alloys. According to the experimental results and microstructural analyses, the trace element Ni exerted only minor effects on the impact toughness of the A356 alloy. On the other hand, V had a strong influence on the impact properties: (i) V-containing sand cast alloys generally absorbed slightly higher impact energies compared to the

[*] Corresponding author. Tel.: +39 0532 974914; fax.: +39 0532 974870
E-mail addresses: daniele.casari@unife.it (D. Casari), thomas.ludwig@hydro.com (T.H. Ludwig), lars.arnberg@ntnu.no (L. Arnberg), mattia.merlin@unife.it (M. Merlin), gian.luca.garagnani@unife.it (G.L. Garagnani).

corresponding A356 base alloys; (ii) in the permanent mould cast alloys, V in solid solution led to a considerable loss of ductility and, as a result, to a significant reduction in the propagation energy, which in turn decreased the total absorbed energy.

KEYWORDS

Aluminium alloys; Casting; Nickel addition; Vanadium addition; Impact toughness; Fracture analysis

INTRODUCTION

The hypoeutectic A356 aluminium foundry alloy (Al-7%Si-0.3%Mg) bases on the quaternary Al-Si-Fe-Mg system and is commonly used in a wide range of automotive, aerospace and other structural applications due to its good castability, high strength to weight ratio, corrosion and wear resistance and ease of recycling.

The mechanical performance of A356 castings depends on their microstructure, which in turn is governed by several parameters such as the alloy chemistry, melt treatment processes (e.g. Sr or Na modification of the Al-Si eutectic and/or grain refinement), cooling rate and heat treatment. The application of a T6 heat treatment is usually performed in the manufacturing process and is a well-established method to increase the strength and ductility of the A356 alloy. In order to obtain an increase in strength, all steps of a T6 heat treatment are required to occur i.e. solution treatment, quenching and artificial aging. The main contribution is obtained from the precipitation of a large amount of fine Mg_2Si particles, which harden the soft α-Al matrix after ageing. On the other hand, a benefit in ductility is generally achieved after the solution treatment stage and is related to necking, fragmentation and subsequent spheroidisation of eutectic Si crystals [1-6]. Eventually, a further optimisation of A356 tensile properties by solution treatment involves a change of the volume fraction of Fe-bearing intermetallic phases, which leads to a replacement of the π-$Al_8FeMg_3Si_6$ with a "Chinese-script" morphology by fine clusters of β-Al_5FeSi needles [7].

Today, the Charpy impact test has become a standard method to evaluate the effect of different process parameters on dynamic fracture toughness of engineering materials. The latter is particularly critical as the demand for high ductility alloys that have to meet specific service conditions, e.g. automotive structural parts, has risen in the last decade. Murali et al. [8] investigated the influence of Mg and Fe on the impact toughness of the AlSi7Mg0.3 alloy. They demonstrated that either the increase of Mg content from 0.32 to 0.65 wt% or the increase of Fe concentration from 0.2 to 0.8 wt% at 0.32 wt% Mg leads to a decrease of the total absorbed energy. Ma et al. [9] also studied the effect of varying Fe concentrations from 0.1 to 0.8 wt% in an A356.2 alloy, showing that a significant reduction in impact toughness occurs when Fe levels are above 0.2 wt% or, in terms of β-intermetallics' size, when the length of β-needles lies within the range of 10 – 50 μm. Shivkumar et al. [10] showed that Sr modification and an increase of the cooling rate improve the impact properties of an A356-T6 alloy. Typical impact energies for unmodified and Sr-modified sand cast impact specimens were reported on the order of 1.5 and 3.0 J. In contrast, permanent mould castings exhibited higher total absorbed energies, on the order of 7 and 13 J in unmodified and Sr-modified alloys, respectively. Merlin et al. [11] applied instrumented Charpy impact test to measure the total absorbed energy of subsize specimens. They stated that casting defects close to the V-notch have a strong detrimental effect on impact toughness. Hence the appearance of casting defects became the predominant parameter masking the influence of the actual microstructural features. Finally, in the authors previous work [12] it was found that the impact properties of a Sr-modified A356 alloy are not directly affected by Ti-B based grain refiners. However, all the grain refiners were reported to produce secondary changes in the microstructural features, increasing both SDAS and β-intermetallics' size. As a direct consequence, a reduction in the total absorbed energies of the grain refined alloys was observed.

Some authors [6, 10] have noticed that there exists a region where the impact energy of a T6 heat treated A356 alloy decreases to a minimum before it increases again. It has been suggested that this behaviour is caused by a compromise between the negative contribution to ductility due to the precipitation of Mg_2Si particles in the α-Al matrix, and the positive contribution associated with the fragmentation and spheroidisation of eutectic Si particles. Solution and homogenisation kinetics that lead to the precipitation of fine Mg_2Si particles during ageing, and consequently to the increase in strength, are faster compared to Si spheroidisation, which usually occurs after prolonged solution heat treatments. Zhang et al. [6] have reported that short solution treatment times in the range of 1.5 – 10 min produce a significant reduction in the impact energy of a low pressure die cast A356 alloy (approximately 3 J and 4 J after 5 min and 20 min, respectively). Even though the alloy is modified with Sr, eutectic Si particles have only begun to spheroidise during these short times, so that the positive contribution to ductility is poor and is completely counteracted by the precipitation of the Mg_2Si strengthening phase. The results of Shivkumar et al. [10] have shown that the previously described scenario is not observed when longer solution times are applied e.g. an impact energy of 2.0 J has been measured for an unmodified permanent mould cast A356 alloy in the as-cast condition, whereas an impact energy of 5.6 J has been reported for the same alloy subjected to 2 h solution treatment, natural ageing for 24 h and artificial ageing at 171 °C for 4 h. Conversely, low impact energy values are maintained over longer solution times in sand cast alloys (i.e. low cooling rates, and hence coarse microstructures), with noticeable differences between Sr-modified and unmodified alloys: the latter usually require further time for the fragmentation and subsequent spheroidisation of eutectic Si particles, so that the corresponding increase in impact energy is postponed.

Finally, Elsebaie et al. [13] have recently investigated the effect of artificial ageing on the impact properties of unmodified and Sr-modified 356 alloys subjected to the same solution heat treatment at 540 °C for 8 h. It has been observed that the ageing at 180 °C for ageing time varying from 2 h to 8 h exerts a negative effect on the impact behaviour of the alloys due to the progressive precipitation of coherent and semi-coherent Mg_2Si particles. Increasing the ageing time to 12 h, however, results in a slight recovery in the impact energies of these alloys. This effect has been attributed to the coarsening and coherency loosening of stable Mg_2Si precipitates, which lead to easy motion of dislocation into α-Al matrix. As a direct consequence, the ductility of the alloy is increased.

Even if many different aspects of A356 impact behaviour have been investigated so far, no data are available in the literature concerning the impact properties of A356 alloy in the presence of Ni and V trace elements. Increasing concentrations of Ni and V impurity elements coming from the manufacturing process of primary aluminium, particularly from the petroleum coke used for the production of anodes for the aluminium electrolysis, have recently arisen as a major issue for the final quality of foundry alloy products [14, 15]. Since currently there are no cost efficient techniques for removal, these elements may constitute a problem for the static and dynamic properties of this widely used alloy.

The aim of the present work is to study the influence of Ni and V trace additions on the impact properties of as-cast and T6 heat treated A356 aluminium foundry alloys in two commercially important casting processes i.e. sand and permanent mould casting. Instrumented Charpy impact tests have been performed and the acquired data have been analysed in terms of maximum load and total absorbed energy. The latter parameter has then been divided into its two main contributions, namely the crack initiation energy, also indicated as energy at maximum load, and the propagation energy, in order to better correlate the experimental findings to the microstructural features of the alloys and to separate the net effects of trace element additions and T6 heat treatment. Moreover, a fractographic analysis has been carried out to investigate the fracture mechanisms and the microstructural features involved in the fracture process.

MATERIALS AND METHODS

A commercial A356 aluminium alloy was used as the base alloy. The as-received alloy ingots were melted in charges of 16 kg each in a boron-nitride coated clay-graphite crucible.

Trace elements were added in the form of Al-10 wt% Ni and Al-10 wt% V master alloys according to the targeted nominal concentrations of 600 and 1000 ppm of Ni and V, respectively. In order to avoid any further interactions, neither Sr nor Na were added as modifier agents. The melting temperature was monitored with the Alspek-H probe and kept constant at 740 °C ± 5 °C. Samples from the three different melts were taken throughout the casting trials and were analysed by optical emission spectroscopy (OES). The chemical composition of the investigated alloys is given in Table 1.

Table 1 Chemical composition (wt%) of the A356 reference alloy and the Ni/V-containing alloys as measured by OES.

Alloy	Addition (ppm)	Si	Fe	Mg	Ni	V	Al
A356	–	7.054	0.092	0.355	0.003	0.007	bal.
A356 + Ni	600	6.902	0.087	0.344	0.061	0.007	bal.
A356 + V	1000	6.992	0.094	0.349	0.003	0.108	bal.

The hydrogen content in the melts was measured in-situ with the Alspek-H probe. Melts were degassed with argon gas in order to reach a hydrogen concentration of 0.08

$mlH_2/100gAl$. The alloys were then poured in both sand and steel moulds. Sand castings were produced using an improved version of the tensile test bar design proposed by Dispinar and Campbell [16]. In this new casting design, the shape of the bars varied from cylindrical to tapered, with diameters increasing gradually from 15 mm (bottom) to 20 mm (top). Permanent mould castings were obtained by pouring the molten alloys into a L-shaped preheated steel die, manufactured according to the UNI 3039 specification. The steel die was kept at a constant temperature of 300°C during the casting trials. This setup yields a cooling rate of 1.2 K/s and 2.5 K/s in the centre of sand cast and permanent mould cast Charpy impact specimens, respectively. Charpy impact specimens were machined according to the UNI EN ISO 148-1 specification (10x10x55 mm). The sand cast impact samples were machined from the upper part of the tapered bars, whereas the permanent mould samples were obtained along the centreline of the feeders (Figure 1).

In order to evaluate the effect of Ni and V in both as-cast and heat treated conditions, specimens from the same casting were subjected to a T6 heat treatment including solutionising at 540 °C for 4 h, followed by quenching in a water bath at 20 °C. Subsequently, the samples were aged at 160 °C for 6 h. As a result, twelve different experimental conditions could be examined (Table 2), and at least 5 samples were tested in each condition.

(Figure 1)

Tab. 2 Experiment matrix

Alloy	Mould	Condition	Alloy Code
A356	Sand	As-cast	A356 – AC
		T6	A356 – T6
A356 + 600 ppm Ni	Sand	As-cast	Ni – AC
		T6	Ni – T6
A356 + 1000 ppm V	Sand	As-cast	V – AC
		T6	V – T6
A356	Permanent Mould	As-cast	A356 PM – AC
		T6	A356 PM – T6
A356 + 600 ppm Ni	Permanent Mould	As-cast	Ni PM – AC
		T6	Ni PM – T6
A356 + 1000 ppm V	Permanent Mould	As-cast	V PM – AC
		T6	V PM – T6

The impact tests were carried out on a CEAST instrumented Charpy pendulum according to the ASTM E-23 specification. Data were acquired using a DAS 8000 analyser. During impact testing, the total absorbed energy (*Wt*) was determined, along with a number of specific parameters such as crack initiation (*Wm*) and propagation (*Wp*) energies and the maximum load required to break the specimens (*Fmax*). *Wm* was calculated as the integral of load-deflection curve from the beginning of the test (i.e. when the pendulum hits the specimen) to the maximum load. This was also defined as the energy at maximum load, whereas the energy absorbed from the maximum load to 2% of the peak value was designated as the propagation energy *Wp*.

After the impact tests, each specimen was sectioned perpendicular to the fracture surface, embedded and prepared with standard metallographic procedures. Microstructures and fracture profiles were then studied with an optical microscope (OM) and scanning electron microscopes (SEM). A detailed investigation of fracture surfaces was performed using a ZEISS EVO MA 15 and a ZEISS ULTRA 55 SEM equipped with EDS microprobe. Leica Application Suite 3.6 was used to measure the SDAS, applying the line intercept method, and the maximum Feret diameter of eutectic

Si particles. As far as SDAS is concerned, between 350 and 500 measurements were performed near the fracture profiles for each sample in order to achieve statistically meaningful results. Regarding eutectic Si, a number of 25 micrographs were observed and more than 5000 particles were measured for each specimen.

RESULTS

Impact properties

It is well established that the shape of both the load-time and the load-deflection curves can give information about the deformation and the fracture history of the impact specimens [17-19]. Qualitative observations of average load-deflection curves (Figure 2a-d) clearly indicate that T6 heat treated alloys exhibit a less ductile fracture behaviour than the as-cast ones. Even if the maximum load increases in both sand cast and permanent mould cast T6 heat treated specimens, the following sharp decrease after the peak load is indicative of unstable crack propagation. The analysis of the corresponding average energy-deflection curves also reveals that generally a smaller amount of energy is absorbed by heat treated specimens.

(Figure 2a-d)

The average values of the impact properties of sand cast and permanent mould cast alloys, as well as their standard deviations, are summarized in Table 3 and Table 4 and shown in Figure 3.

Table 3 Impact properties of the sand cast base and Ni/V-containing alloys. *Fmax* is the maximum load required to break the specimens; *Wt* is the total absorbed energy; *Wm* is the energy at maximum load; *Wp* is the propagation energy.

Alloy Code	Fmax [N]	Wt [J]	Wm [J]	Wp [J]
A356 – AC	2704 ± 86	1.32 ± 0.05	0.45 ± 0.04	0.87 ± 0.05
A356 – T6	3987 ± 93	1.05 ± 0.08	0.52 ± 0.08	0.53 ± 0.08
Ni – AC	2818 ± 62	1.31 ± 0.06	0.45 ± 0.09	0.86 ± 0.06
Ni – T6	4186 ± 76	1.22 ± 0.06	0.67 ± 0.05	0.55 ± 0.03
V – AC	2810 ± 62	1.51 ± 0.06	0.71 ± 0.17	0.80 ± 0.14
V – T6	4133 ± 100	1.25 ± 0.08	0.68 ± 0.05	0.57 ± 0.04

Table 4 Impact properties of the permanent mould cast base and Ni/V-containing alloys. *Fmax* is the maximum load required to break the specimens; *Wt* is the total absorbed energy; *Wm* is the energy at maximum load; *Wp* is the propagation energy.

Alloy Code	Fmax [N]	Wt [J]	Wm [J]	Wp [J]
A356 PM – AC	3122 ± 132	1.84 ± 0.20	0.79 ± 0.07	1.05 ± 0.13
A356 PM – T6	4362 ± 184	1.52 ± 0.13	0.81 ± 0.09	0.71 ± 0.06
Ni PM – AC	2971 ± 63	1.68 ± 0.17	0.78 ± 0.02	0.91 ± 0.16
Ni PM – T6	4401 ± 318	1.51 ± 0.22	0.78 ± 0.10	0.73 ± 0.14
V PM – AC	3021 ± 143	1.54 ± 0.15	0.82 ± 0.05	0.72 ± 0.12
V PM – T6	4598 ± 148	1.60 ± 0.11	0.88 ± 0.08	0.72 ± 0.13

(Figure 3a-d)

It is obvious, that the heat treatment has a key influence on the impact properties of the alloys. Firstly, it leads to an increase of the maximum loads required to break the specimens *Fmax* (Figure 3a); secondly, it leads to a general decrease in propagation energies *Wp* (Figure 3c). However, considering the plots of the energy at maximum load *Wm* (Figure 3b) and the total absorbed energy *Wt* (Figure 3d), it is evident that the T6 heat treatment alone is not sufficient to affect the impact properties. Other parameters such as the SDAS and eutectic Si particles size must be considered as well.

The addition of the trace element Ni to an A356 base alloy exerts a very small effect on the total absorbed energy (*Wt*) of as-cast samples (- *AC*). On the other hand, V has a strong influence. It increases the average total absorbed energy of the sand cast specimens, whereas the same parameter is reduced up to 20% in permanent mould cast samples. Considering the deconvolution of total absorbed energy into its two main contributions, namely *Wm* and *Wp*, it is observed that Ni does not lead to any significant change in any of the impact parameters compared to the average values of the corresponding sand and permanent mould cast base alloys. In particular, since the scatter of *Wp* values for the *Ni PM – AC* alloy is large and includes the *A356 PM – AC* *Wp* average value, it is not possible to determine a clear influence of Ni addition on the propagation energy. The effect of V addition is less ambiguous. Although the scatter of *Wm* values for the sand cast alloy is large, a sharp increase in energy at maximum load is detected (Figure 3b, *V – AC vs. A356 – AC*). However, the trace element V has a detrimental effect on the propagation energy of permanent mould impact specimens (Figure 3c, *V PM – AC vs. A356 PM – AC*). It yields a decrease of *Wp* from 1.05 to 0.72 J.

For the case of the T6 heat treated alloys (*– T6*), the net influence of the trace elements Ni and V on the total absorbed energy was only observed in the sand cast specimens. The partition of this parameter into its two main contributions showed that both Ni and V increased the energy at maximum load, whereas propagation energy remained unaffected. Conversely, the alloys poured into the permanent mould did not show any significant variation of the average *Wt* values, compared to the corresponding T6 base alloy.

It is worth noting that an inversion in the relative contributions of *Wm* and *Wp* to *Wt* generally occurs between as-cast and T6 heat treated sand cast and permanent mould cast alloys (Figure 4). As shown, the contribution of the propagation energy to the total absorbed energy is higher than *%Wm* for the reference alloys, the Ni-containing alloys and the sand cast V added alloy in as-cast condition (*A356 – AC, Ni – AC, V – AC, A356 PM – AC*, *Ni PM – AC*), whereas the remaining alloys generally show an opposite tendency. Hence, it is evident that several parameters need to be considered to completely describe the impact behaviour of sand cast and permanent mould cast alloys in both as-cast and T6 heat treated conditions.

(Figure 4)

<u>Microstructural and fractographic observations</u>

The as-cast microstructures of reference alloys and alloys with Ni and V additions comprise soft α-Al dendrites and acicular eutectic Si particles (Figure 5). During heat treatment some of the unmodified Si particles undergo necking, separate into segments, and then spheroidise and coarsen. However most of them still show an elongated acicular shape in both sand cast and permanent mould cast alloys (Figures 5b and 5d).

(Figure 5a-d)

Various intermetallic phases such as π-$Al_8FeMg_3Si_6$, β-Al_5FeSi, Mg_2Si and Ni-bearing compounds can be observed in the interdendritic regions depending on the composition of the as-cast alloy (Figure 6). The β-Al_5FeSi phase appears in the form of randomly distributed needles, whereas the π-$Al_8FeMg_3Si_6$ and Mg_2Si intermetallics have a "Chinese-script" morphology. Microstructural observations also reveal an increased amount of the latter two phases in the V-containing alloy, as can be noted from the comparison of Figure 6a and Figure 6c. As shown in Figure 6b, Ni-based intermetallic compounds precipitate as discrete particles or with a "Chinese-script" morphology. EDS spot measurements identify these phases as Al_3Ni and Al_9FeNi (Figure 7). This is consistent with the microstructural investigations carried out by Ludwig et al. [20] in a commercial purity A356 alloy with Ni concentration ranging between 300 and 600 ppm.

The average size of the intermetallics decreases in permanent mould cast alloys due to the higher cooling rate that was obtained with this casting technique.

(**Figure 6a-c**)

(**Figure 7**)

Fine scale "Chinese-script" Mg_2Si intermetallics are not observed after solution heat treatment as reported in a number of previous studies [2, 7, 13, 21]. This provides evidence that they completely dissolve in the α-Al matrix for the given solution time and temperature of 4 h and 540 °C, respectively. Additionally, the fraction of the π-$Al_8FeMg_3Si_6$ phase diminishes by gradual dissolution of Mg and Si into the matrix and is to a some extent replaced by a Mg-free phase similar in composition to the β-Al_5FeSi phase (Figure 8a) in the base and V-containing alloys, and to the Al_9FeNi phase (Figure 8b) in the alloys added with Ni, as also observed by means of EDS (Figure 8c). Conversely, acicular β-Al_5FeSi intermetallic phases formed during solidification are generally not affected by solution heat treatment [7], as well as Al_9FeNi intermetallics in the Ni-containing alloys, whereas Al_3Ni undergoes gradual spheroidisation. Apart from the precipitation of hardening Mg_2Si particles into α-Al matrix, the subsequent ageing heat treatment at 160 °C does not produce any further variation in the other microstructural features of the investigated alloys.

(**Figure 8a-c**)

Quantitative microstructural analysis of the investigated alloys was only performed by measuring the secondary dendrite arm spacing (SDAS) and the size distribution of eutectic Si particles, since the intermetallic compounds were scarcely found on the fracture profiles and surfaces of the impact specimens. As given in Table 5, average

SDAS values of permanent mould cast alloys are lower than those of the corresponding sand cast alloys. This can be attributed to the higher cooling rate obtained in permanent mould casting as compared to sand casting. Furthermore, it is worthwhile noticing that a T6 heat treatment has no influence on the SDAS within the limits of the experimental scatter. This is in excellent agreement with the observations by other authors [10,18,22,23] concluding that the SDAS is generally independent of the heat treatment even when extended solutionising times were applied to the investigated Al-Si-Mg alloys.

Table 5 Average values and standard deviations of the measured microstructural features for each experimental condition.

Alloy Code	SDAS [µm]	Si particles Ave. Max. Feret Diameter [µm]
A356 – AC	59.8 ± 5.6	126.0 ± 7.0
A356 – T6	62.6 ± 9.9	119.5 ± 4.8
Ni – AC	60.1 ± 5.5	139.1 ± 9.4
Ni – T6	60.5 ± 6.5	125.0 ± 7.3
V – AC	59.7 ± 6.2	138.1 ± 10.3
V – T6	60.6 ± 6.1	112.9 ± 8.2
A356 PM – AC	50.1 ± 6.8	100.4 ± 11.7
A356 PM – T6	51.7 ± 6.9	73.0 ± 7.4
Ni PM – AC	51.5 ± 5.8	107.7 ± 11.4
Ni PM – T6	53.1 ± 7.4	75.6 ± 17.7
V PM – AC	47.1 ± 7.0	103.5 ± 8.4
V PM – T6	49.0 ± 5.6	74.9 ± 12.5

In addition to the abovementioned effects on the intermetallic compounds and on the precipitation behaviour of Mg_2Si hardening particles, the T6 heat treatment mainly affects the size and shape of eutectic Si particles (Figure 5). Therefore, the size class containing the largest eutectic Si particles in terms of Feret diameter (50) was recorded for each sample and the average values for each experimental condition (i.e. base and Ni/V-containing sand cast and permanent mould cast alloys in both as-cast and T6 heat treated conditions) were calculated and considered as an indirect index of the heat treatment efficiency based on the change of the morphology of the eutectic Si from coarse acicular to fragmented and spheroidised.

It can be observed from the values summarized in Table 5, that a T6 heat treatment has a larger effect on the permanent mould cast alloys compared to alloys made by sand casting owing to the higher cooling rate. This led to the precipitation of finer micro-constituents, and in consequence these particles were easier to fragment and spheroidise during solution heat treatment, i.e. the Si crystals were moderately refined due to the higher velocity of the advancing eutectic solid-liquid interface. This observation further substantiates the observations of Wang et al. [24] and correlates well with the model proposed by Ogris et al. [25]. Corresponding size distributions of eutectic Si particles shown in Figures 9a and 9b clearly indicate an higher tendency to necking and fragmentation of eutectic Si crystals for the T6 heat treated permanent mould cast base alloy (*A356 PM – T6*) compared to the sand cast alloy (*A356 – T6*). Similar observations can be made for alloys containing higher concentrations of Ni or V.

(Figure 9a,b)

However, as mentioned previously, a large fraction of eutectic Si particles still possess an elongated acicular morphology. This demonstrates that, in the absence of Sr or Na as modifier agents, the selected solution heat treatment holding time is insufficient to obtain complete necking and spheroidisation of the eutectic Si phase. Therefore several areas with high stress concentration in the vicinity of acicular Si crystals maintain in all the T6 heat treated alloys investigated in this study.

Figures 10a-d show details of fracture profiles for the A356 reference alloy, considering that similar fracture paths can also be detected in the alloys with added Ni and V. Intercrystalline fracture of acicular eutectic Si crystals was the cause for fracture initialisation. Once a critical number of fractured particles is reached, the principal crack is formed by the local linkage of adjacent microcracks. They propagate following a preferential quasi-cleavage path along eutectic Si particles. Note that intermetallics are rarely found along the fracture profiles, thus indicating a Si-driven crack propagation, with a predominantly transgranular fracture mode. Occasionally, small intergranular contributions to fracture were detected in the permanent mould cast alloys (Figure 10c). This is probably due to the presence of a locally smaller SDAS compared to the total average values measured for the corresponding alloys. This is in good agreement with previous results [22, 24,26], demonstrating that for coarser microstructures (i.e. large SDAS) a strong interaction occurs during deformation between the slip bands generated in the secondary dendrite arms (also called dendrite cells) and the dense array of Si particles in the surrounding interdendritic regions. The resulting significant particle cracking and local linkage of microcracks along the interdendritic regions provides an easy path for transgranular crack propagation. On the contrary, smaller SDAS and Si particles make dendrite cell boundaries more discontinuous. As a consequence, transgranular fracture becomes more difficult; fracture then propagates throughout the grain boundaries, which offer an alternative continuous path.

No differences in fracture paths are observed between as-cast and T6 heat treated alloys. As already pointed out, even when some acicular Si particles fragmented and spheroidised during solution heat treatment, most of them still maintained an elongated acicular morphology and imposed a great influence on fracture propagation.

For the sake of simplicity, Figures 11a-d show only the fracture surfaces of the A356 reference alloys. A careful examination of the surfaces confirms a Si-driven quasi-cleavage fracture mode. As mentioned before, the solution heat treatment decreases the size of Si flakes (Figures 11b and 11d). However, the typical characteristics of brittle fracture remain even in alloys where fragmentation and spheroidisation effects seem to be more pronounced (e.g. *A356 PM – T6, Ni PM – T6, V PM – T6*).

(**Figure 10a-d**)

(**Figure 11a-d**)

DISCUSSION

Impact properties of the base and Ni/V-containing as-cast alloys

It is generally accepted that the fracture process of Al-Si alloys consists of three stages, namely (i) particle cracking, (ii) microcrack formation and growth, and (iii) linkage of microcracks [22]. These stages are controlled by the microstructure in terms of size and shape of eutectic Si particles and intermetallic phases, and their clustering around the secondary arms of α-Al dendrites. When the SDAS is large, the microcrack linking process occurs more easily along the cell boundaries leading to a low-energy transgranular fracture mode. In contrast, small SDAS microstructures generally account for higher ductility and impact properties due to a linking process between the microcracks. This involves fracture along the more irregular grain boundary region, i.e. an intergranular fracture mode [12]. It is worth noting that an increase in particle size also increases the probability of fracture, which generally leads to a lower fracture stress [24, 27].

The present results are consistent with these findings. Low total absorbed energy average values (Wt < 2 J) are observed for the investigated as-cast alloys (the *– AC* alloys in Tables 3 and 4) due to the large SDAS and the resulting significant amount of large acicular eutectic Si particles between secondary arms (Table 5), which provide an easier path for a low-energy transgranular crack propagation. The slight increase in the total absorbed energies of the reference and Ni-containing permanent mould cast alloys in as-cast condition (*A356 PM – AC*, *Ni PM – AC*) reveals the moderate beneficial effect of a finer microstructure leading to local intergranular contributions to fracture. Since intermetallic compounds are scarcely found on the fracture profiles and surfaces (Figures 10 and 11), their influence on impact properties is considered negligible compared to the SDAS and the size and shape of eutectic Si particles, indicating a Si-driven crack propagation. These observations are in excellent agreement with the findings of Kobayashi and Niinomi on the impact toughness of as-cast Al-Si alloys, which was reported to be primarily related to SDAS and eutectic Si rather than other second-phase particles such as intermetallic compounds [28]. According to the microstructural analysis, this also holds for Ni-bearing intermetallic compounds implying that the addition of the trace element Ni exerts no effect on the impact toughness of both sand cast and permanent mould cast A356 aluminium alloys. Conversely, the comparison between the reference alloys and the corresponding V-containing alloys (*A356 – AC vs. V – AC*, *A356 PM – AC vs. V PM – AC*) in terms of total absorbed energy shows that V has a significant effect on the impact behaviour of the A356 alloy. In particular, the influences of V addition on the total absorbed energies of *V – AC* and *V PM – AC* alloys need to be analysed. The amount of V added in the present study is close to its maximum solubility in the α-Al matrix (≈ 0.1 wt%) [29]. Hence a solid solution strengthening effect occurs. This enhances the strength of the matrix (*Fmax, Wm*), and at the same time reduces its ductility (*Wp*) due to the blockage of dislocation movement and the subsequent dislocation pile-ups. As a result, the microcrack linking process that follows the fracture of eutectic Si particles advances faster, especially in case of coarse microstructures. Therefore, two simultaneous effects occur and interact in V-containing as-cast alloys. In the sand cast alloys (*V – AC vs. A356 – AC*) the higher average value of *Wt* is due to the increase in energy at maximum load linked to solid solution strengthening, whereas the ductility reduction (i.e. the decrease in propagation energy) related to V appears to be moderate and within the experimental scatter. This appears to be reasonable considering the well-established detrimental influence of a coarse microstructure (large SDAS and eutectic Si particles) on the impact properties of A356 alloy [10,13,28,30]. On the contrary, in the permanent mould cast alloys (*V PM – AC vs. A356 PM – AC*), the smaller SDAS and the slightly refined eutectic Si particles have a prevalent effect on *Fmax* and *Wm* compared to V strengthening: as it can be observed in Table 4 and Figure 3b, the alloys show similar values of these parameters (*Fmax* ≈ 3100 N, *Wm* ≈ 0.80 J). However, it appears that the influence of V on the ductility loss (*Wp*) increases as the microstructure becomes finer, thus contributing to a decrease of the total absorbed energy.

<u>Impact properties of the base and Ni/V-containing T6 heat treated alloys</u>

It is evident from the average values of total absorbed energies listed in Tables 3 and 4 that the selected T6 heat treatment has a negative effect on the impact toughness of all the investigated alloys compared to the as-cast condition. These results are in good agreement with previous investigations, which indicated a noticeable decrease of the impact toughness of unmodified A356 alloys in T6 condition [10, 13]. Although Elsebaie et al. [13] studied unnotched impact specimens, it is worth noticing that this reduction was observed in both experiments with alloys with a large SDAS (45 ± 48 μm). Additionally, Shivkumar et al. [10] reported that increasing solution heat treatment times led to a recovery of the impact toughness.

These findings can be explained as follows. Owing to the fact that the propagation of microcracks in an A356 alloy is governed by the ductility of α-Al matrix, an increase of the relative volume fraction of the matrix is definitely beneficial for the impact properties. This effect can be achieved by the addition of Sr or Na, resulting in the modification of the eutectic Si from a coarse acicular structure to a fine fibrous morphology, and/or the application of a solution treatment [10]. Both treatments produce an increase in inter-particle spacing. However, different to chemical modification, the solutionising locally increases the relative volume fraction of the α-Al matrix due to necking, spheroidisation and coarsening of eutectic Si particles [6, 11, 13, 30, 31]. Without the addition of modifier elements and for insufficient solution treatment holding times and temperatures, the relative volume fraction of the α-Al matrix does not change substantially, and the linkage of microcracks proceeds predominantly along the cell boundaries of alloys with a large SDAS (i.e. low-energy transgranular fracture). Therefore, no significant improvement of the impact toughness is observed [10].

Furthermore, the ageing process that follows the solutionising step may become detrimental for the impact properties, thus causing a decrease in total absorbed energy [13]. A T6 heat treatment is normally applied to increase the strength of Al-Si-Mg alloys by the precipitation of fine coherent Mg_2Si particles. These dispersoids harden the α-Al matrix at the expense of ductility. In fact, they impose an obstacle for dislocation movement leading to a pile up, and consequently contribute significantly to the increase of the strength of the α-Al matrix [32]. Despite this improvement, the matrix is prone to fracture more easily. As a result, when the cracking of acicular Si particles begins, the following microcrack linking process is faster and leads to a lower amount of absorbed energy for fracture propagation. Hence, it is believed that a third parameter, namely the precipitation of coherent Mg_2Si particles, controls the impact energies of the alloys in T6 condition together with SDAS and eutectic Si particles size and shape.

These two opposing effects of an ageing treatment on strength and ductility of the investigated alloys can clearly be observed in Figure 3. On the one hand, the T6 heat treatment increases the maximum load required to fracture (*Fmax*); on the other hand, it leads to a general decrease in propagation energies (*Wp*) compared to the as-cast alloys. However, it is worth noticing that two different minimum levels of *Wp* are reached for the T6 heat treated sand cast and permanent mould cast alloys (Figure 3c). It is suggested that the increase in *Wp* values for the permanent mould cast alloys is related to their finer microstructures in terms of SDAS and eutectic Si particles. In fact, it is already established that the Mg concentration in the α-Al matrix approaches the saturation limit within 30 minutes at 540 °C in alloys with low Mg concentration (0.3, 0.4 wt%), due to the dissolution of the Mg_2Si phase and the transformation of the π-Fe to the β-Fe intermetallic [7, 21, 33]. Since all the investigated alloys were subject to the same T6 heat treatment, which also included an extended solutionising time, i.e. 4 h, the same ductility loss was obtained. Hence, only the smaller SDAS and the slightly refined eutectic Si particles account for the further improvements of the propagation energies. However, these increases remain moderate because of the inadequate solution heat treatment holding time, that did not lead to sufficiently fragmented and spheroidised eutectic Si particles.

For the energy at maximum load (Figure 3b), a small strengthening effect related to Mg_2Si precipitation was observed in the sand cast base alloy (*A356 – T6*). Conversely, as described before for the permanent mould cast alloys in as-cast condition, it is the finer microstructure that appears to control the energy at maximum load of the T6 heat treated permanent mould cast alloys (*A356 PM – T6, Ni PM – T6, V PM – T6*) rather than the hardening Mg_2Si phase itself. Moreover, no further increases in *Wm* are observed for these alloys compared to the as-cast ones. This supports the hypothesis of an insufficient fragmentation and spheroidisation of eutectic Si particles.

The large increase in *Wm* for the sand cast Ni-containing alloy (*Ni – T6*) is not completely understood yet and requires further investigations. However, since the decrease in propagation energy is larger than the increase in energy at maximum load, the T6 heat treatment produces an overall reduction in total absorbed energy to fracture.

The presence of V in the α-Al matrix represents another parameter affecting the impact toughness of the T6 heat treated sand cast alloy (*V – T6*). It is noted in Figure 3b, that the solid solution strengthening effect due to the presence of V produces a significant increase in *Wm*, similar to that observed in the as-cast alloy (*V – AC*). No further improvements of the energy at maximum load originating from the precipitation of Mg_2Si particles are observed. Nevertheless, it is believed that the combination of the ageing treatment and the coarse microstructure decreases the propagation energy of the alloy (Figure 3c). However, as the beneficial effect of V is predominant, the V-containing alloy in T6 condition absorbs a slightly higher impact energy compared to the corresponding reference alloy (*V – T6 vs. A356 – T6* in Figure 3d). For the case of permanent mould casting, similarly to the *V PM – AC* alloy, the presence of trace element V in the α-Al matrix yields a significant decrease in the propagation energy of the corresponding T6 heat treated alloy (*V PM – T6*). In contrast to the T6 heat treated reference and Ni-containing alloys, it appears that the minimum ductility of the α-Al matrix has already been achieved by V solid solution strengthening, so that the additional precipitation of coherent Mg_2Si particles does not reduce the ductility any further.

The variations of the percentage contributions to the total absorbed energy (Figure 4) are due to these complex and interconnected mechanisms, which act simultaneously during the fracture process and govern the impact behaviour of sand cast and permanent mould cast alloys in both as-cast and T6 heat treated conditions.

CONCLUSIONS

The impact behaviour of base and Ni- or V-containing A356 alloys in as-cast and T6 heat treated conditions has been studied by testing notched specimens obtained from both sand and permanent mould castings. The main observations can be summarised as follows:

1. Low total absorbed energy average values (Wt < 2 J) are observed for all the alloys under investigation. Slightly higher impact energies are reported for the permanent mould cast alloys compared to sand cast specimens.

2. Intermetallic particles are rarely found on the fracture surfaces of the alloys, thus indicating a Si-driven quasi-cleavage crack propagation, with a predominant low-energy transgranular fracture mode. Occasionally, local intergranular contributions to fracture are detected in the permanent mould cast alloys, most likely due to the finer microstructure that forms due to the higher cooling rate. No differences are observed between as-cast and T6 heat treated alloys: even if acicular Si particles undergo fragmentation and spheroidisation during solution heat treatment, most of them still show an elongated acicular shape and maintain a great influence on fracture propagation.

3. With respect to as-cast alloys (– *AC*), the addition of the trace element Ni to an A356 base alloy exerts a minor effect on the total absorbed energy (Wt).

However, this parameter is affected by the addition of V: while V increases the average total absorbed energy of the sand cast specimens, *Wt* of permanent mould cast samples is decreased up to 20%. This is due to an interaction between V solid solution strengthening and the resultant microstructure, the former being the prevalent parameter when the SDAS and Si particles are large (i.e. in sand cast alloys, *V – AC vs. A356 – AC*). In the permanent mould cast alloys (*V PM – AC vs. A356 PM – AC*), the effect of a smaller SDAS and slightly reduced eutectic Si particles on *Fmax* and *Wm* dominates over the V solid solution strengthening. However, the ductility loss (*Wp*) attributed to V in solid solution leads to a decrease in the total absorbed energy.

4. The T6 heat treatment (*– T6*) has a key influence on the increase of the maximum load required to fracture the specimens, *Fmax*, as well as on the reduction of the propagation energy *Wp*. These opposite effects occur because of the precipitation of fine coherent Mg_2Si particles, which lead to a hardening of the α-Al matrix at the expense of ductility. In addition, the microstructure affects the impact properties of the T6 heat treated alloys to some extent: higher *Wm* and *Wp* average values are reported for the permanent mould cast alloys compared to the corresponding sand cast ones.

5. The overall influence of Ni on the impact properties of the T6 heat treated A356 alloy is negligible. However V exerts a strong effect on the impact toughness of T6 heat treated sand cast and permanent mould cast alloys (*V – T6*, *V PM – T6*): in the former case it yields an increase of the energy at maximum load, whereas in the latter it significantly reduces the propagation energy.

Our investigation suggests that the presence of V, rather than Ni, needs to be taken into account in order to meet the specific service requirements in terms of impact toughness, in particular when structural parts are manufactured with different casting processes and subsequently subjected to a T6 heat treatment. It seems that the same detrimental influence on the impact toughness of a permanent mould cast unmodified A356 alloy is obtained either by adding the trace element V or via the application of T6 heat treatment. However, when these two factors are present simultaneously, their effects do not add up. Conversely, both the hardening of α-Al matrix due to V solid solution strengthening and the ductility loss caused by Mg_2Si precipitation are observed in case of sand cast T6 heat treated alloys (*V – T6*). Therefore, in the light of these results, more investigations are necessary in order to better understand the interactions between these microstructural features, particularly for the case of a Sr-modified A356 alloy, where mechanical properties are further improved by eutectic Si modification.

ACKNOWLEDGEMENTS

This research project was supported by the "Bando Giovani Ricercatori – Fondi 5x1000 anno 2010 e Fondi Unicredit 2013" of the University of Ferrara. In addition, the authors gratefully acknowledge Hydro Aluminium AS (Norway) for financial support. Thanks are also due to Hermann Hovland from Sør-Norge Aluminium AS (Norway) for the generous supply of master alloys and to Arne Nordmark and Kurt Sandaunet for the help during the manufacture of castings.

REFERENCES

[1] D. Apelian, S. Shivkumar, and G. Sigworth, Fundamental aspects of heat treatment of cast Al-Si-Mg alloys, *AFS Trans.*, 97, 1989, p 727-742, in English.

[2] E. Sjölander, and S. Seifeddine, The heat treatment of Al-Si-Cu-Mg casting alloys, *J. Mater. Process. Technol.*, 210(10), 2010, p 1249-1259, in English.

[3] K.T. Kashyap, S. Murali, K.S. Raman, K.S.S. Murthy, Casting and heat treatment variables of Al-7Si-Mg alloy, *Mater. Sci. Technol.*, 9(3), 1993, p 189-204, in English.

[4] L. Pedersen, and L. Arnberg, The Effect of Solution Heat Treatment and Quenching Rates on Mechanical Properties and Microstructures in AlSiMg Foundry Alloys, *Metall. Mater. Trans. A*, 32(3), 2001, p 525-532, in English.

[5] M. Zhu, Z. Jian, G. Yang, and Y. Zhou, Effects of T6 heat treatment on the microstructure, tensile properties, and fracture behavior of the modified A356 alloys, *Mater. Des.*, 36, 2012, p 243-249, in English.

[6] D.L. Zhang, L.H. Zheng, and D.H. StJohn, Effect of a short solution treatment time on microstructure and mechanical properties of modified Al-7wt.%Si-0.3wt.%Mg alloy, *J. Light Met.*, 2(1), 2002, p 27-36, in English.

[7] J.A. Taylor, D.H. St John, L. Zheng, G.A. Edwards, J. Barresi, and M.J. Couper, Solution Treatment Effects in Al-Si-Mg Casting Alloys: Part I. Intermetallic Phases, *Alum. Trans.*, 4-5, 2001, p 95-110, in English.

[8] S. Murali, K.S. Raman, and K.S.S. Murthy, Effect of magnesium, iron (impurity) and solidification rates on the fracture toughness of Al-7Si-0.3Mg casting alloy, *Mater. Sci. Eng. A*, 151(1), 1992, p 1-10, in English.

[9] Z. Ma, F.H. Samuel, A.M. Samuel, H.W. Doty, and S. Valtierra, Effect of Fe Content and Cooling Rate on the Impact Toughness of Cast 319 and 356 Aluminum Alloys, *AFS Trans.* 111, 2003, p 255-266, in English.

[10] S. Shivkumar, L. Wang, and C. Keller, Impact properties of A356-T6 Alloys, *J. Mater. Eng. Perform.*, 3(1), 1994, p 83-90, in English.

[11] M. Merlin, G. Timelli, F. Bonollo, and G.L. Garagnani, Impact behaviour of A356 alloy for low-pressure die casting automotive wheels, *J. Mater. Process. Technol.*, 209(2), 2009, p 1060-1073, in English.

[12] D. Casari, M. Merlin, and G.L. Garagnani, A comparative study on the effects of three commercial Ti-B-based grain refiners on the impact properties of A356 cast aluminium alloy, *J. Mater. Sci.*, 48(12), 2013, p 4365-4377, in English.

[13] O. Elsebaie, A.M. Samuel, and F.H. Samuel, Effects of Sr-modification, iron-based intermetallics and aging treatment on the impact toughness of 356 Al-Si-Mg alloy, *J. Mater. Sci.*, 46(9), 2011, p 3027-3045.

[14] G. Jha, S. Ningileri, X. Li, and R. Bowers, The Challenge of Effectively Utilizing Trace Elements/Impurities in a Varying Raw Materials Market, *Light Metals 2013,* B. Sadler, Ed., TMS, 2013, p 929-934.

[15] J. Grandfield, L. Sweet, C. Davidson, J. Mitchell, A. Beer, S. Zhu, X. Chen, and M. Easton, An initial assessment of the effects of increased Ni and V content in A356 and AA6063 alloys, *Light Metals 2013*, B. Sadler, Ed., TMS, 2013, p 39-45.

[16] D. Dispinar, and J. Campbell, Porosity, hydrogen and bifilm content in Al alloy castings, *Mater. Sci. Eng. A*, 528(10-11), 2011, p 3860-3865, in English.

[17] Z. Li, A.M. Samuel, F.H. Samuel, C. Ravindran, H.W. Doty, and S. Valtierra, Parameters controlling the performance of AA319-type alloys Part II. Impact properties and fractography, *Mater. Sci. Eng. A*, 367(1-2), 2004, p 111-122, in English.

[18] N.D. Alexopoulos, and A. Stylianos, Impact mechanical behaviour of Al-7Si-Mg (A357) cast aluminum alloy. The effect of artificial aging, *Mater. Sci. Eng. A*, 528(16-20), 2011, p 6303-6312, in English.

[19] N.D. Alexopoulus, A. Stylianos, and J. Campbell, Dynamic fracture toughness of Al-7Si-Mg (A357) aluminum alloy, *Mech. Mater.*, 58, 2013, p 55-68, in English.

[20] T.H. Ludwig, P.L. Schaffer, and L. Arnberg, Influence of Some Trace Elements on Solidification Path and Microstructure of Al-Si Foundry Alloys, *Metall. Mater. Trans. A*, 44(8), 2013, p 3783-3796, in English.

[21] J.A. Taylor, D.H. StJohn, J. Barresi, and M.J. Couper, Influence of Mg Content on the Microstructure and Solid Solution Chemistry of Al-7%Si-Mg Casting Alloys During Solution Treatment, *Mater. Sci. Forum.*, 331-337, 2000, p 277-282, in English.

[22] Q.G. Wang, Microstructural Effects on the Tensile and Fracture Behavior of Aluminum Casting Alloys A356/357, *Metall. Mater. Trans. A*, 34(12), 2003, p 2887-2899, in English.

[23] Y. Harada, S. Tamura, and S. Kumai, Effects of High-Temperature Solutionizing on Microstructure and Tear Toughness of A356 Cast Aluminum Alloy, *Mater. Trans.*, 52(5), 2011, p 848-855, in English.

[24] Q.G. Wang, and C.H. Cáceres, The fracture mode in Al-Si-Mg casting alloys, *Mater. Sci. Eng. A*, 241(1-2), 1998, p 72-82, in English.

[25] E. Ogris, A. Wahlen, H. Luchinger, and P.J. Uggowitzer, On the silicon spheroidization in Al-Si alloys, *J. Light Met.* 2(4), 2002, p 263-269, in English.

[26] C.H. Cáceres, C.J. Davidson, and J.R. Griffiths, The deformation and fracture behaviour of an Al-Si-Mg casting alloy, *Mater. Sci. Eng. A*, 197(2), 1995, p 171-179, in English.

[27] W.H. Hunt Jr, J.R. Brockenbrough, P.E. Magnusen, An Al-Si-Mg composite model system: Microstructural effects on deformation and damage evolution, *Scripta Metall. Mater.*, 25(1), 1991, p 15-20, in English.

[28] T. Kobayashi, and M. Niinomi, Fracture Toughness and fatigue characteristics of aluminum casting alloy, *J.JAPAN Inst. Met.*, 41, 1991, p 398-405, in Japanese.

[29] N.A. Belov, D.G. Eskin, and A.A. Aksenov, Multicomponent phase diagrams: applications for commercial aluminum alloys, 1st ed., Elsevier Science, 2005, p 379-380.

[30] F. Paray, B. Kulunk, and J.E. Gruzleski, Impact properties of Al-Si foundry alloys, *Int. J. Cast Metals Res.*, 13, 2000, p 17-37, in English.

[31] S.S. Sreeja Kumari, R.M. Pillai, T.P.D. Rajan, and B.C. Pai, Effects of individual and combined additions of Be, Mn, Ca and Sr on the solidification behaviour, structure and mechanical properties of Al-7Si-0.3Mg-0.8Fe alloy, *Mater. Sci. Eng. A* 460-461, 2007, p 561-573, in English.

[32] G.E. Dieter, Mechanical Metallurgy, 3rd ed., WILEY-WCH Verlag, 1988, Chap. 6.

[33] D. Lados, D. Apelian, and L. Wang, Solution Treatment Effects on Microstructure and Mechanical Properties of Al-(1 to 13 Pct)Si-Mg Cast Alloys, *Metall. Mater. Trans. B*, 42(1), 2011, p 171-180, in English.

FIGURE CAPTIONS

Fig. 1 Castings obtained from: a) sand mould; b) permanent mould. The black rectangles mark the areas from where the Charpy specimens c) were machined.

Fig. 2 Load-deflection and energy-deflection average curves for the different experimental conditions: a) sand mould, as-cast; b) sand mould, T6; c) permanent mould, as-cast; d) permanent mould, T6.

Fig. 3 Impact properties of the sand cast and permanent mould cast reference and Ni/V-containing alloys in as-cast and T6 conditions: a) maximum load *Fmax*; b) energy at maximum load *Wm*, c) propagation energy *Wp*; d) total absorbed energy *Wt*. The standard deviation is given as *error bars*.

Fig. 4 Relative contribution of *Wm* and *Wp* to the total absorbed energy during crack nucleation and propagation for the different experimental conditions. The standard deviation is given as *error bars*.

Fig. 5 Microstructures of the investigated A356 base alloys showing α-Al dendrites and an Al-Si eutectic mixture in the interdendritic regions: a) sand mould, as-cast; b) sand mould, T6; c) permanent mould, as-cast; d) permanent mould, T6. Similar features are observed for the Ni/V-containing alloys.

Fig. 6 BSE images showing intermetallic phases in the a) A356 reference, b) Ni-containing and c) V-containing alloys. The images are taken from sand cast samples in as-cast condition.

Fig. 7 BSE image of Ni-bearing intermetallics with different morphologies detected in the interdendritic regions of the sand cast Ni-containing alloy in as-cast condition. The chemical composition from a coarse flake-like particles as measured by EDS indicates the precipitation of the Al_9FeNi phase.

Fig. 8 BSE images of the Mg-free intermetallic compounds (in white) precipitated from the π-$Al_8FeMg_3Si_6$ phase after T6 heat treatment: a) β-Al_5FeSi; b) Al_9FeNi, occasionally forming a layered structure on the π-phase; c) Close-up view of the Ni-containing intermetallics with the corresponding EDS spectrum.

Fig. 9 Size distributions of eutectic Si crystals for a) sand cast and b) permanent mould cast base alloys.

Fig. 10 BSE images of the fracture profile of the A356 reference alloy showing the Si-driven nature of impact fracture: a) sand mould, as-cast; b) sand mould, T6; c) permanent mould, as-cast; d) permanent mould, T6. Smaller SDAS are observed in permanent mould cast alloys implying the occurrence of local intergranular fracture c).

Fig. 11 SEM images of fracture surfaces of the A356 reference alloy showing the Si-driven nature of impact fracture: a) sand mould, as-cast; b) sand mould, T6; c) permanent mould, as-cast; d) permanent mould, T6. Note that the typical characteristics of fragile fracture still remain even in alloys where the effect of solution heat treatment appears to be more pronounced d).

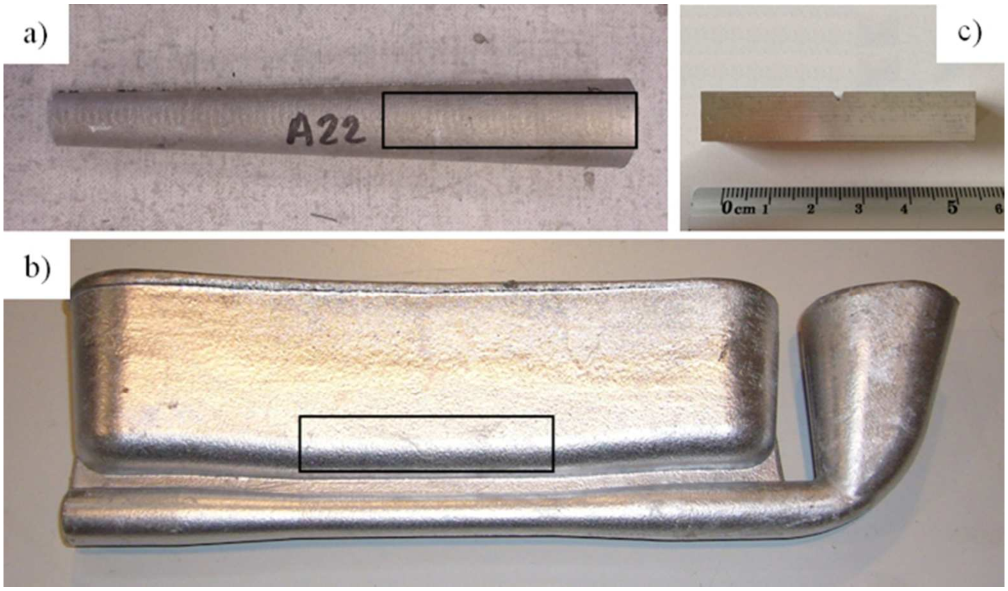

Fig. 1 Castings obtained from: a) sand mould; b) permanent mould. The black rectangles mark the areas from where the Charpy specimens c) were machined.
61x36mm (300 x 300 DPI)

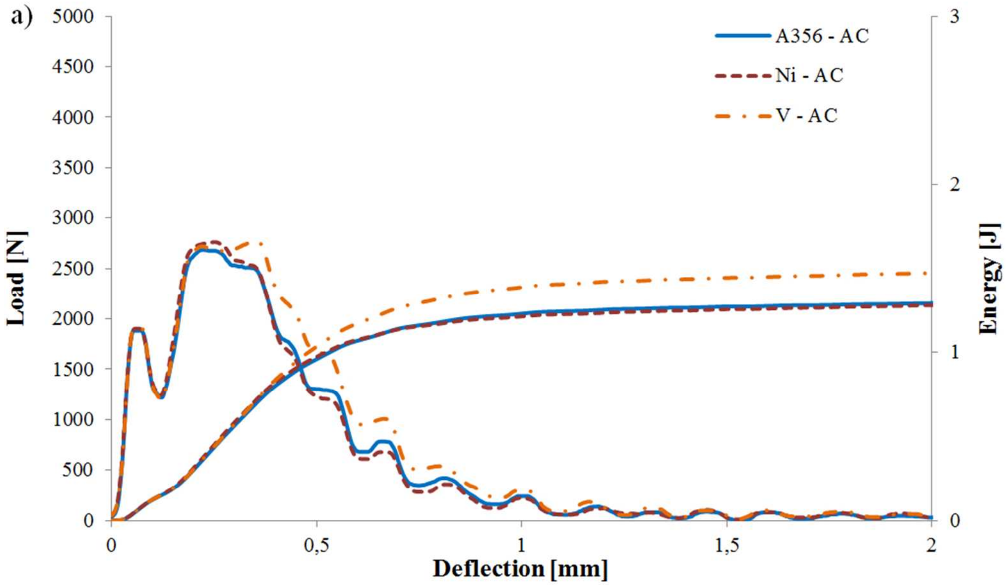

Fig. 2 Load-deflection and energy-deflection average curves for the different experimental conditions: a) sand mould, as-cast; b) sand mould, T6; c) permanent mould, as-cast; d) permanent mould, T6.
86x50mm (300 x 300 DPI)

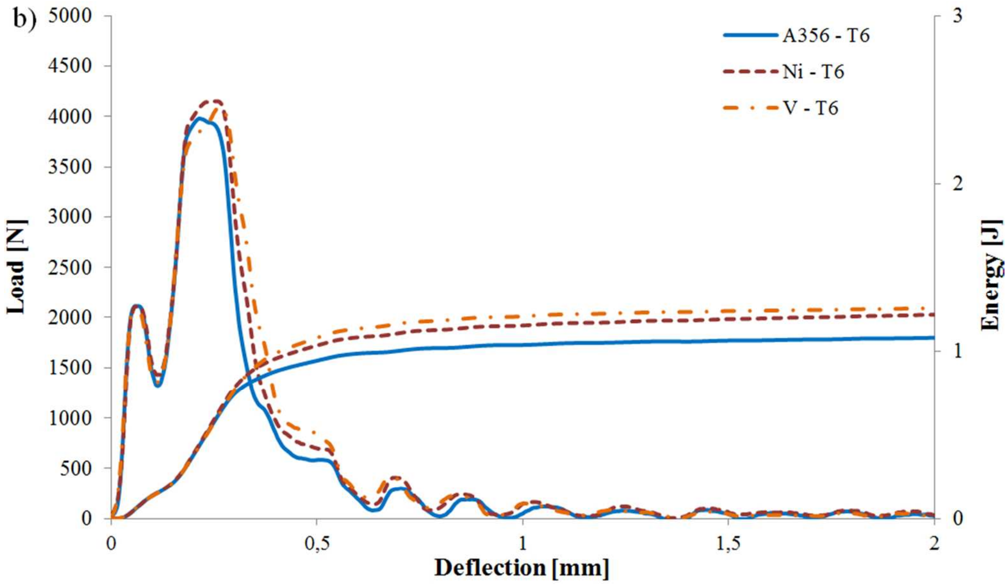

Fig. 2 Load-deflection and energy-deflection average curves for the different experimental conditions: a) sand mould, as-cast; b) sand mould, T6; c) permanent mould, as-cast; d) permanent mould, T6.
86x50mm (300 x 300 DPI)

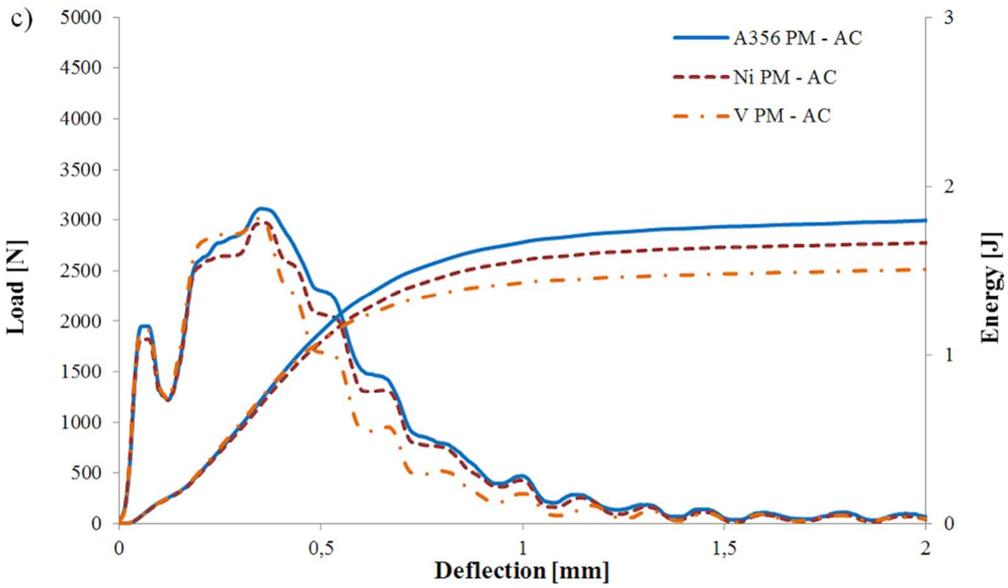

Fig. 2 Load-deflection and energy-deflection average curves for the different experimental conditions: a) sand mould, as-cast; b) sand mould, T6; c) permanent mould, as-cast; d) permanent mould, T6.
86x50mm (300 x 300 DPI)

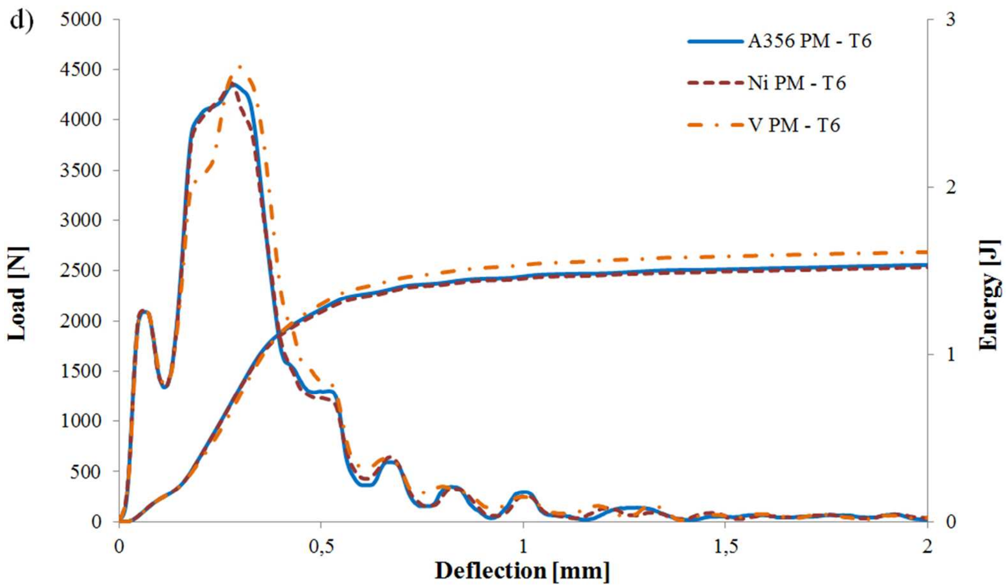

Fig. 2 Load-deflection and energy-deflection average curves for the different experimental conditions: a) sand mould, as-cast; b) sand mould, T6; c) permanent mould, as-cast; d) permanent mould, T6.
86x50mm (300 x 300 DPI)

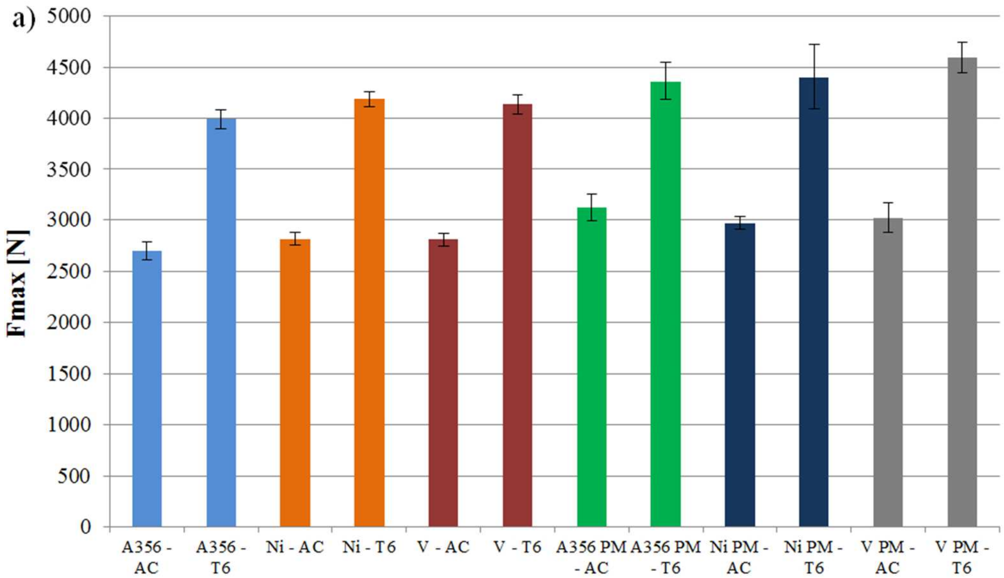

Fig. 3 Impact properties of the sand cast and permanent mould cast reference and Ni/V-containing alloys in as-cast and T6 conditions: a) maximum load Fmax; b) energy at maximum load Wm, c) propagation energy Wp; d) total absorbed energy Wt. The standard deviation is given as error bars.
80x47mm (300 x 300 DPI)

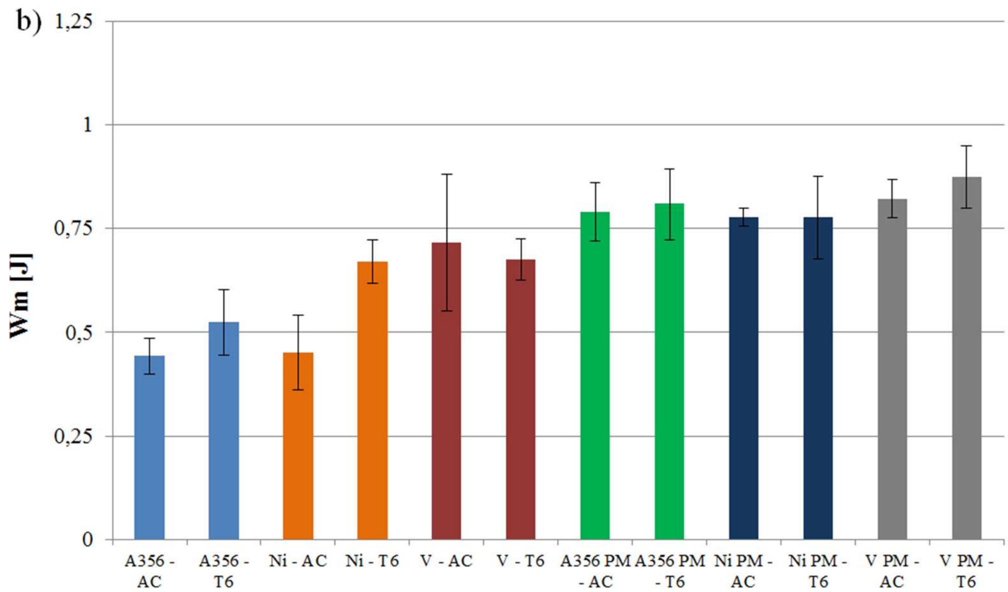

Fig. 3 Impact properties of the sand cast and permanent mould cast reference and Ni/V-containing alloys in as-cast and T6 conditions: a) maximum load Fmax; b) energy at maximum load Wm, c) propagation energy Wp; d) total absorbed energy Wt. The standard deviation is given as error bars.
80x47mm (300 x 300 DPI)

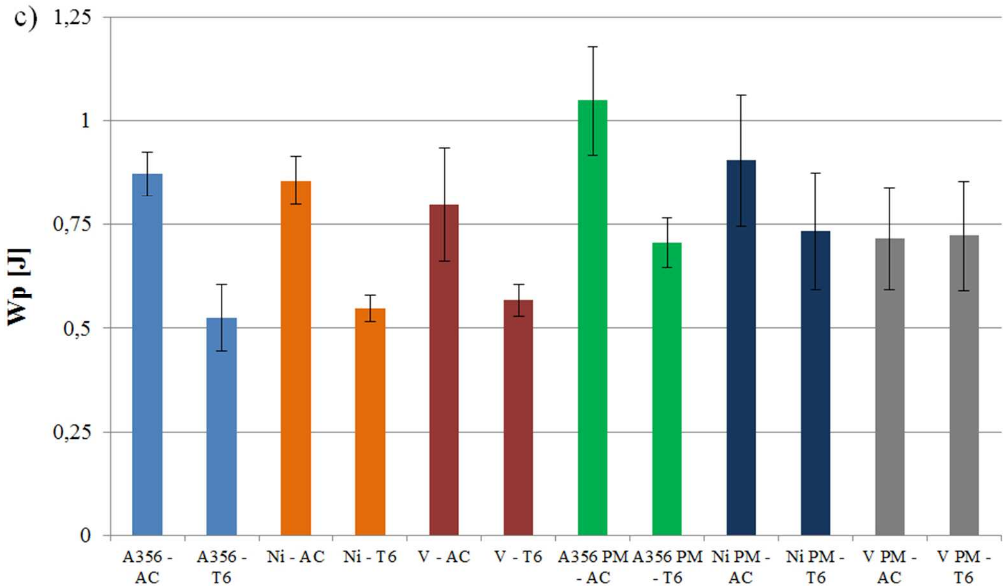

Fig. 3 Impact properties of the sand cast and permanent mould cast reference and Ni/V-containing alloys in as-cast and T6 conditions: a) maximum load Fmax; b) energy at maximum load Wm, c) propagation energy Wp; d) total absorbed energy Wt. The standard deviation is given as error bars.
252x147mm (96 x 96 DPI)

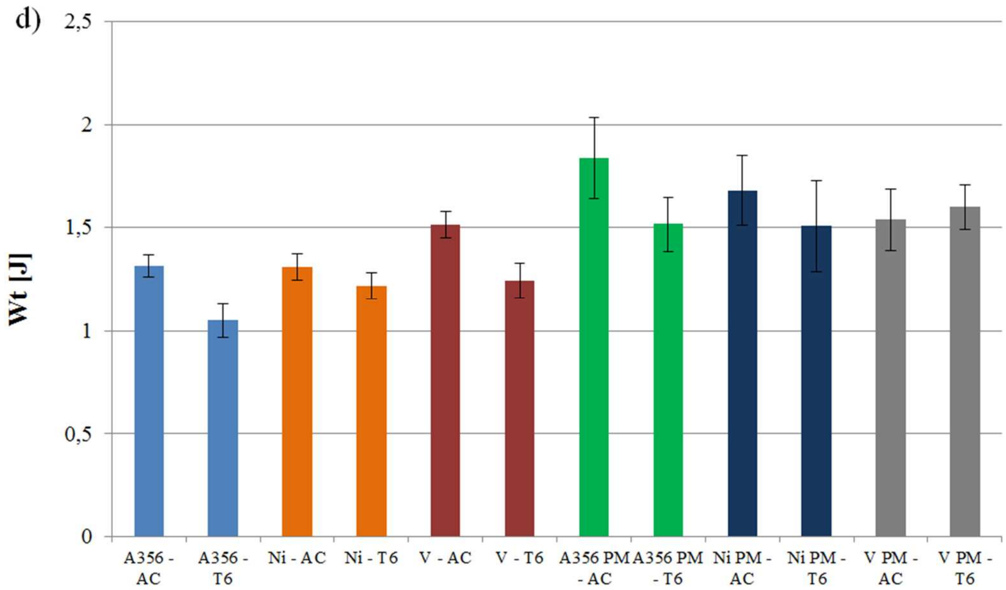

Fig. 3 Impact properties of the sand cast and permanent mould cast reference and Ni/V-containing alloys in as-cast and T6 conditions: a) maximum load Fmax; b) energy at maximum load Wm, c) propagation energy Wp; d) total absorbed energy Wt. The standard deviation is given as error bars.
80x47mm (300 x 300 DPI)

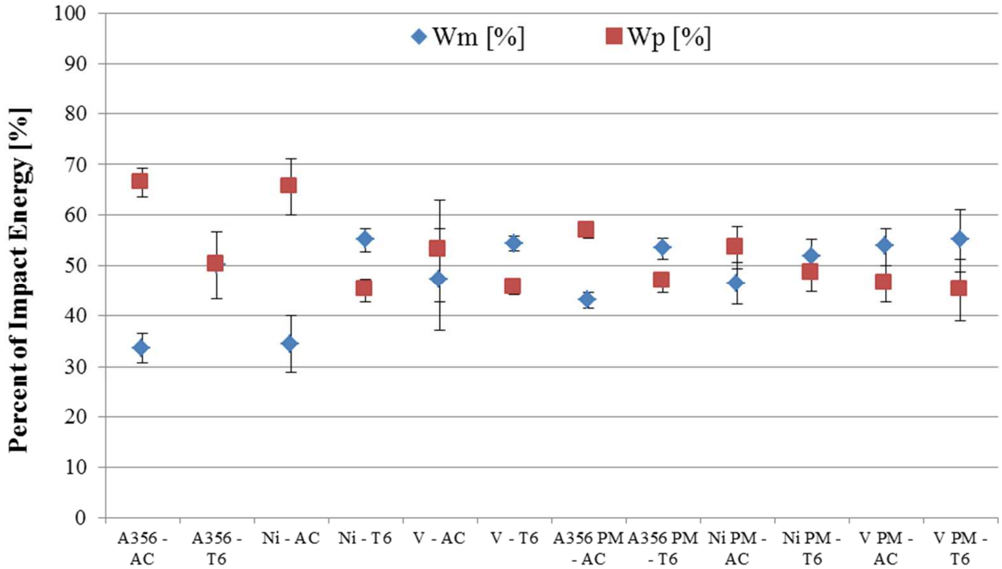

Fig. 4 Relative contribution of Wm and Wp to the total absorbed energy during crack nucleation and propagation for the different experimental conditions. The standard deviation is given as error bars.
80x47mm (300 x 300 DPI)

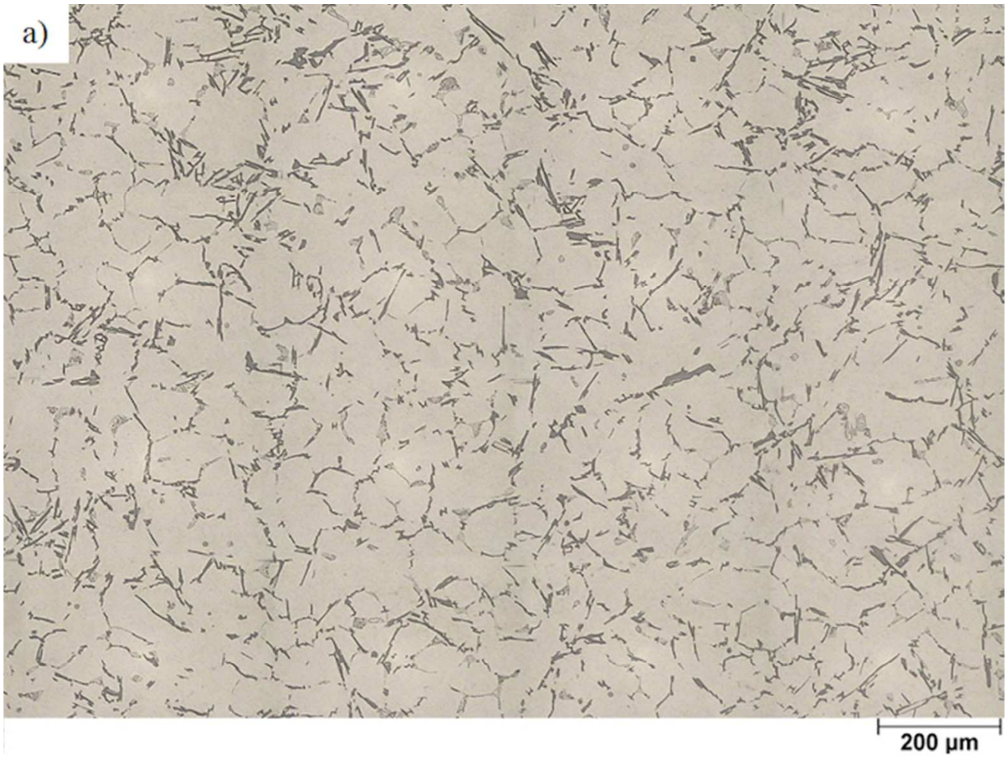

Fig. 5 Microstructures of the investigated A356 base alloys showing α-Al dendrites and an Al-Si eutectic mixture in the interdendritic regions: a) sand mould, as-cast; b) sand mould, T6; c) permanent mould, as-cast; d) permanent mould, T6. Similar features are observed for the Ni/V-containing alloys.
60x45mm (300 x 300 DPI)

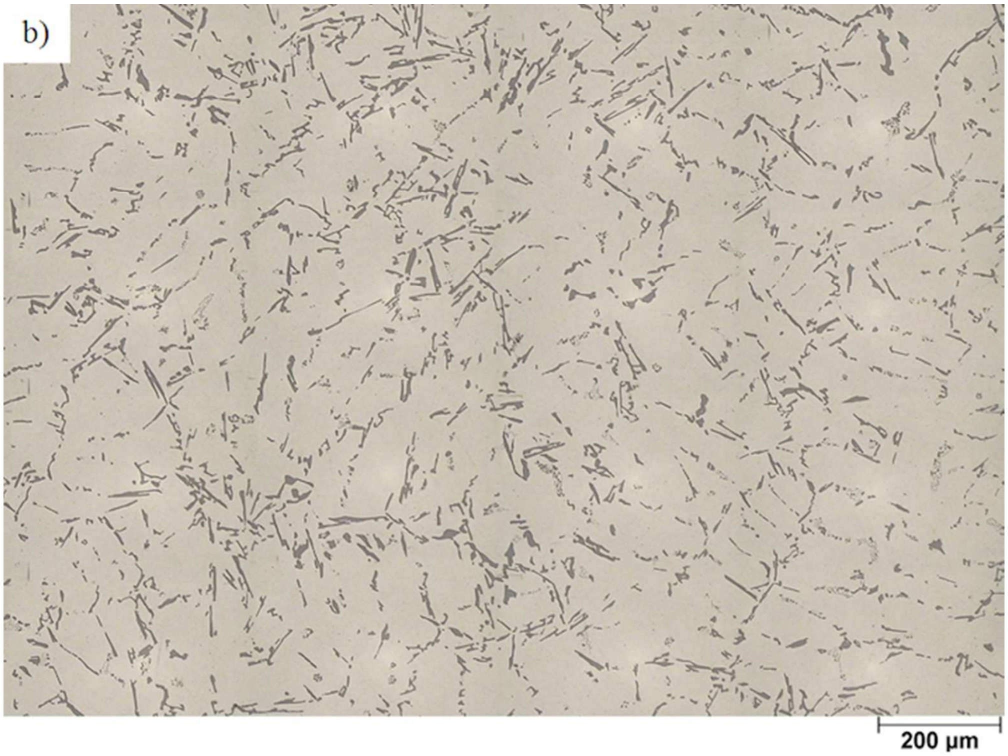

Fig. 5 Microstructures of the investigated A356 base alloys showing α-Al dendrites and an Al-Si eutectic mixture in the interdendritic regions: a) sand mould, as-cast; b) sand mould, T6; c) permanent mould, as-cast; d) permanent mould, T6. Similar features are observed for the Ni/V-containing alloys.
60x45mm (300 x 300 DPI)

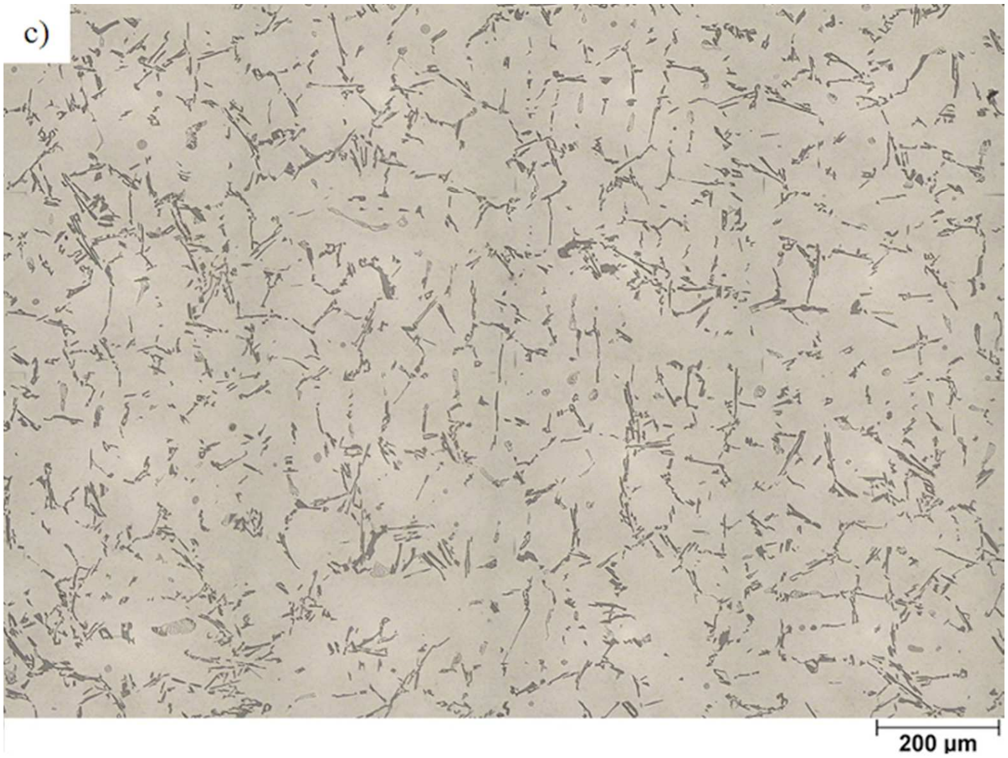

Fig. 5 Microstructures of the investigated A356 base alloys showing α-Al dendrites and an Al-Si eutectic mixture in the interdendritic regions: a) sand mould, as-cast; b) sand mould, T6; c) permanent mould, as-cast; d) permanent mould, T6. Similar features are observed for the Ni/V-containing alloys.
60x45mm (300 x 300 DPI)

Fig. 5 Microstructures of the investigated A356 base alloys showing α-Al dendrites and an Al-Si eutectic mixture in the interdendritic regions: a) sand mould, as-cast; b) sand mould, T6; c) permanent mould, as-cast; d) permanent mould, T6. Similar features are observed for the Ni/V-containing alloys.
60x45mm (300 x 300 DPI)

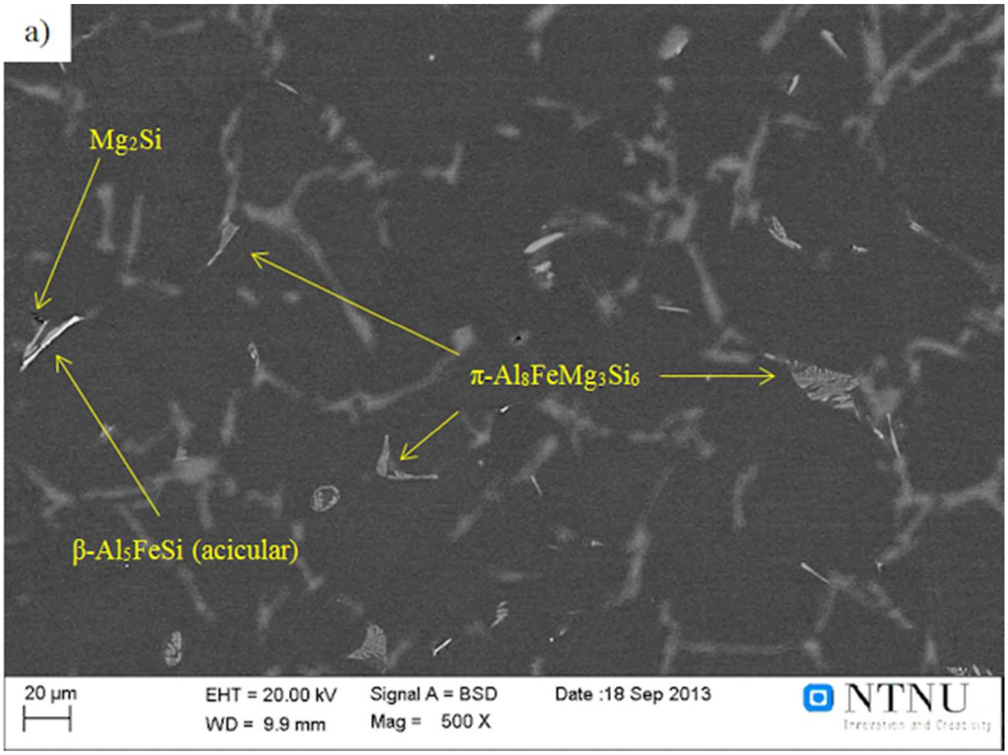

Fig. 6 BSE images showing intermetallic phases in the a) A356 reference, b) Ni-containing and c) V-containing alloys. The images are taken from sand cast samples in as-cast condition.
53x40mm (300 x 300 DPI)

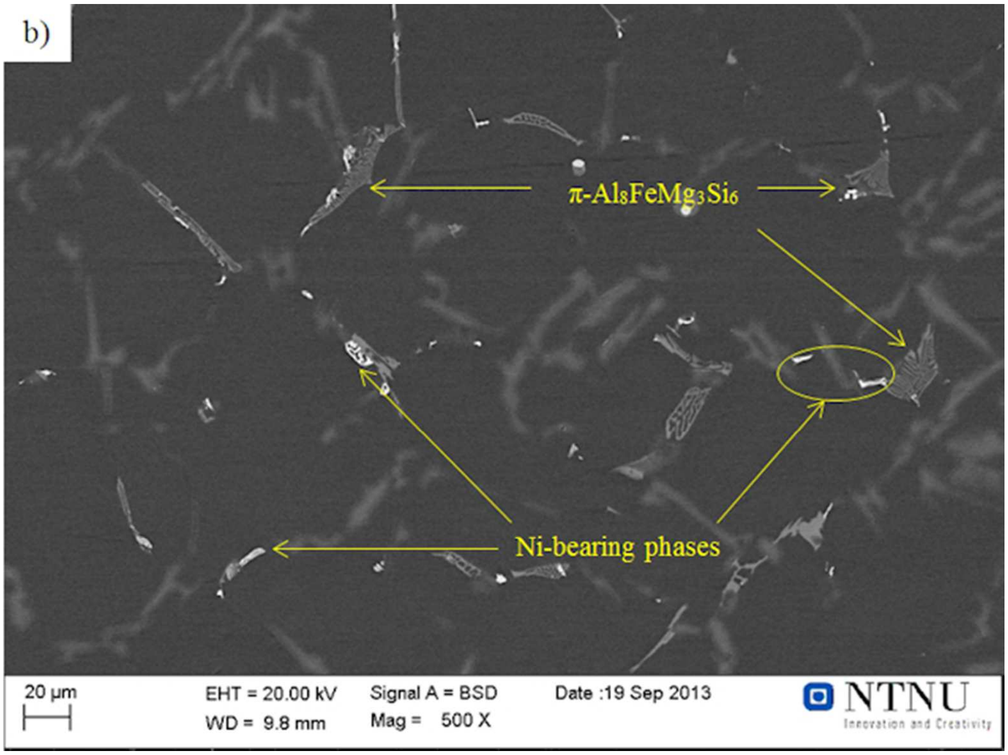

Fig. 6 BSE images showing intermetallic phases in the a) A356 reference, b) Ni-containing and c) V-containing alloys. The images are taken from sand cast samples in as-cast condition.
53x40mm (300 x 300 DPI)

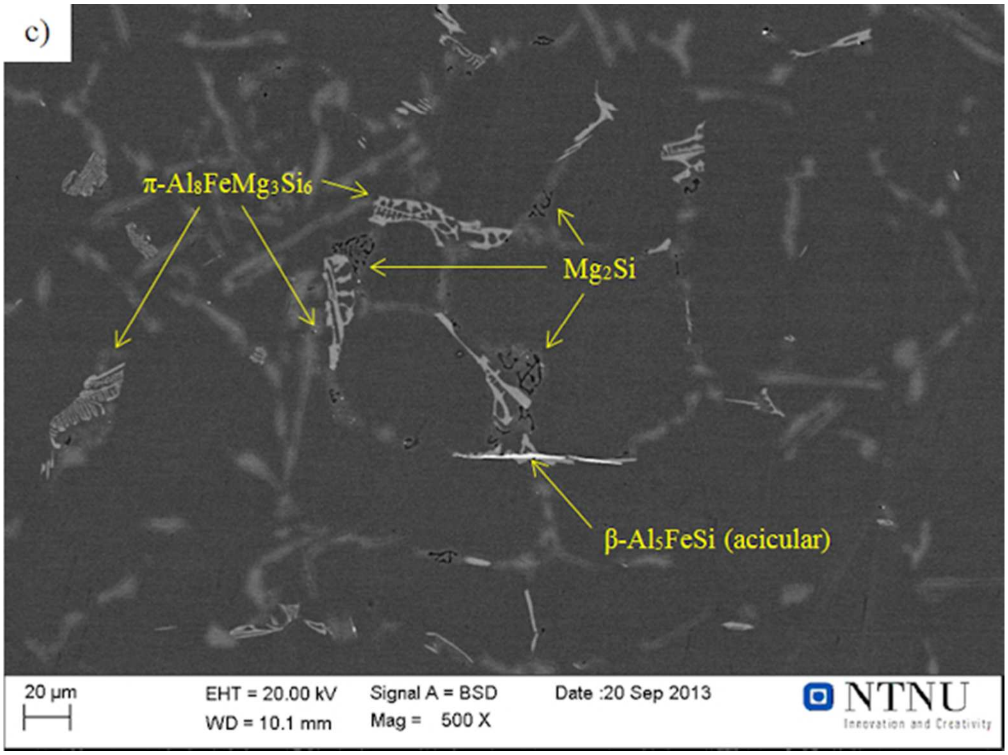

Fig. 6 BSE images showing intermetallic phases in the a) A356 reference, b) Ni-containing and c) V-containing alloys. The images are taken from sand cast samples in as-cast condition.
53x40mm (300 x 300 DPI)

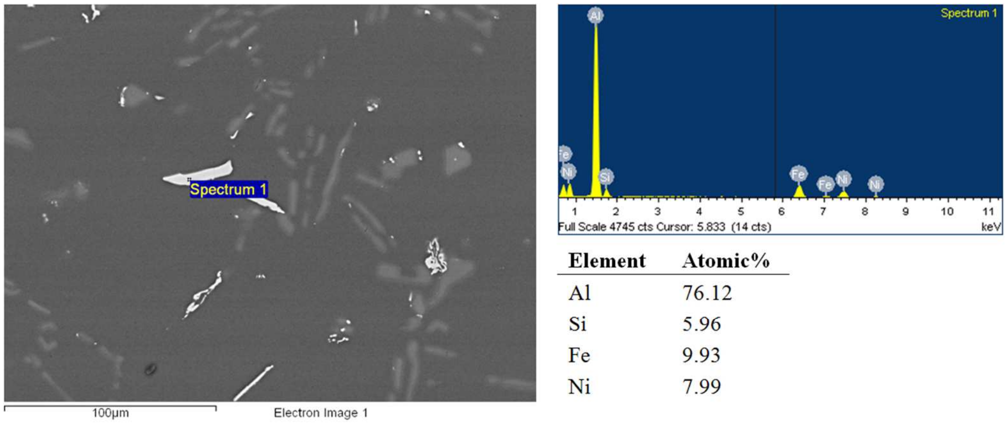

Element	Atomic%
Al	76.12
Si	5.96
Fe	9.93
Ni	7.99

Fig. 7 BSE image of Ni-bearing intermetallics with different morphologies detected in the interdendritic regions of the sand cast Ni-containing alloy in as-cast condition. The chemical composition from a coarse flake-like particles as measured by EDS indicates the precipitation of the Al9FeNi phase.
105x44mm (300 x 300 DPI)

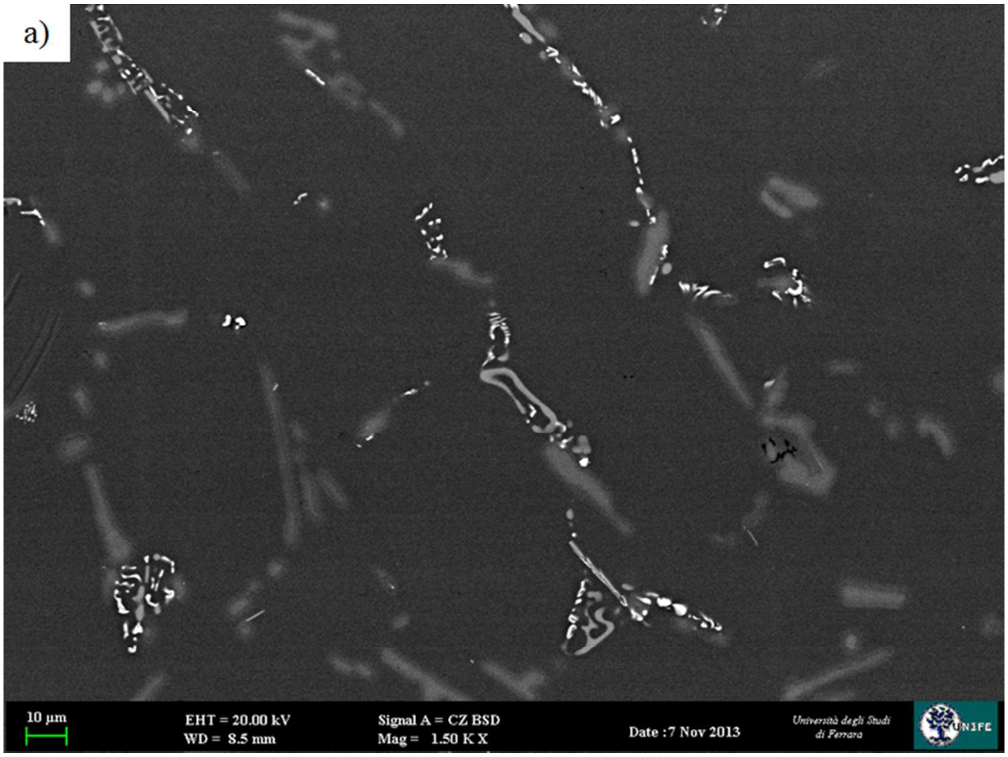

Fig. 8 BSE images of the Mg-free intermetallic compounds (in white) precipitated from the π-$Al_8FeMg_3Si_6$ phase after T6 heat treatment: a) β-Al_5FeSi; b) Al_9FeNi, occasionally forming a layered structure on the π-phase; c) Close-up view of the Ni-containing intermetallics with the corresponding EDS spectrum.
66x50mm (300 x 300 DPI)

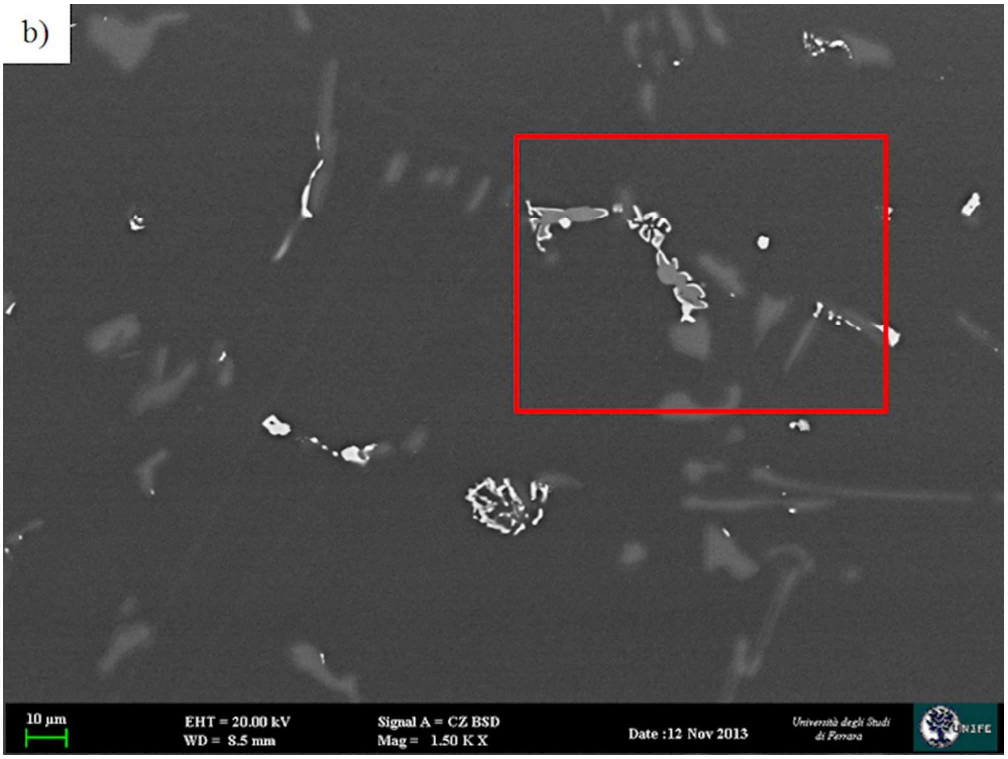

Fig. 8 BSE images of the Mg-free intermetallic compounds (in white) precipitated from the π-$Al_8FeMg_3Si_6$ phase after T6 heat treatment: a) β-Al_5FeSi; b) Al_9FeNi, occasionally forming a layered structure on the π-phase; c) Close-up view of the Ni-containing intermetallics with the corresponding EDS spectrum.

67x50mm (300 x 300 DPI)

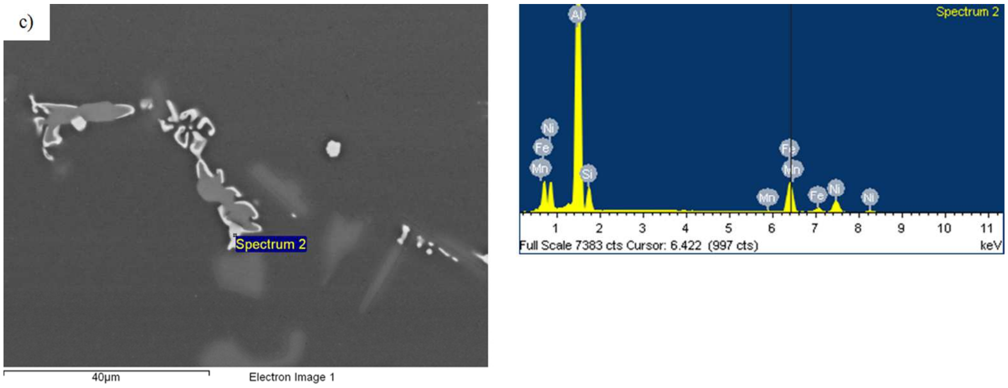

Fig. 8 BSE images of the Mg-free intermetallic compounds (in white) precipitated from the π-Al8FeMg3Si6 phase after T6 heat treatment: a) β-Al5FeSi; b) Al9FeNi, occasionally forming a layered structure on the π-phase; c) Close-up view of the Ni-containing intermetallics with the corresponding EDS spectrum.
341x130mm (96 x 96 DPI)

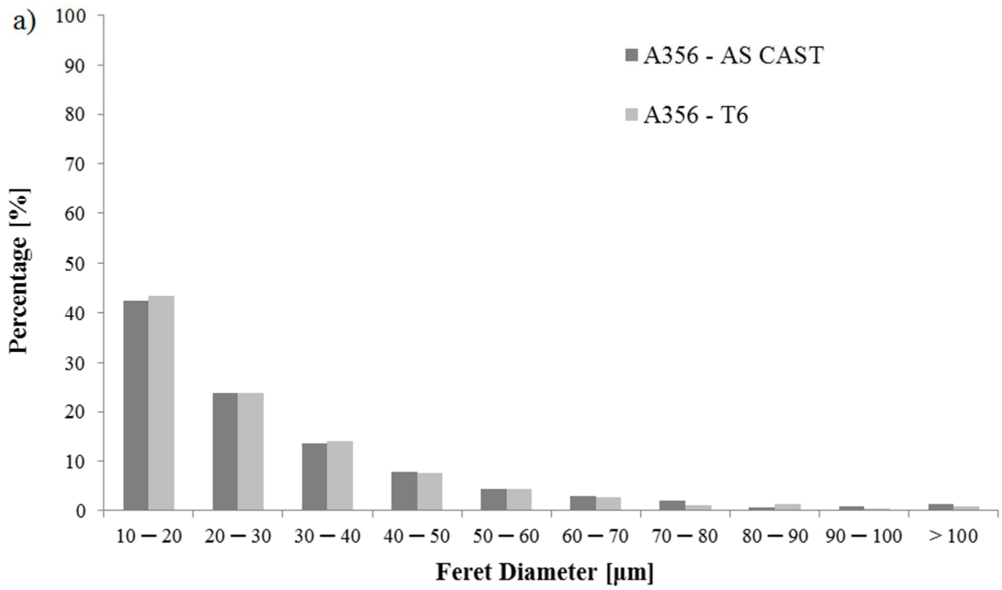

Fig. 9 Size distributions of eutectic Si crystals for a) sand cast and b) permanent mould cast base alloys.
74x43mm (300 x 300 DPI)

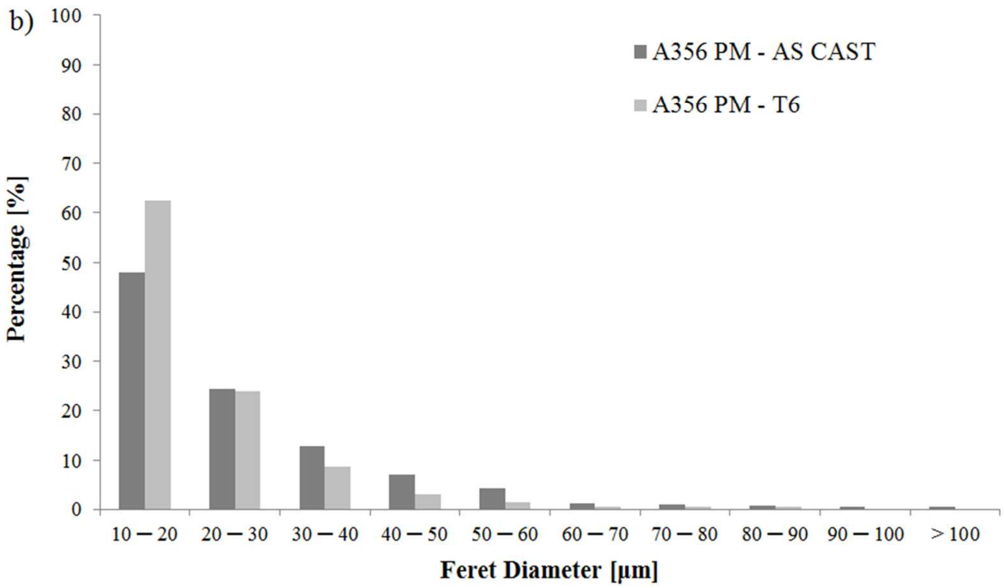

Fig. 9 Size distributions of eutectic Si crystals for a) sand cast and b) permanent mould cast base alloys.
74x43mm (300 x 300 DPI)

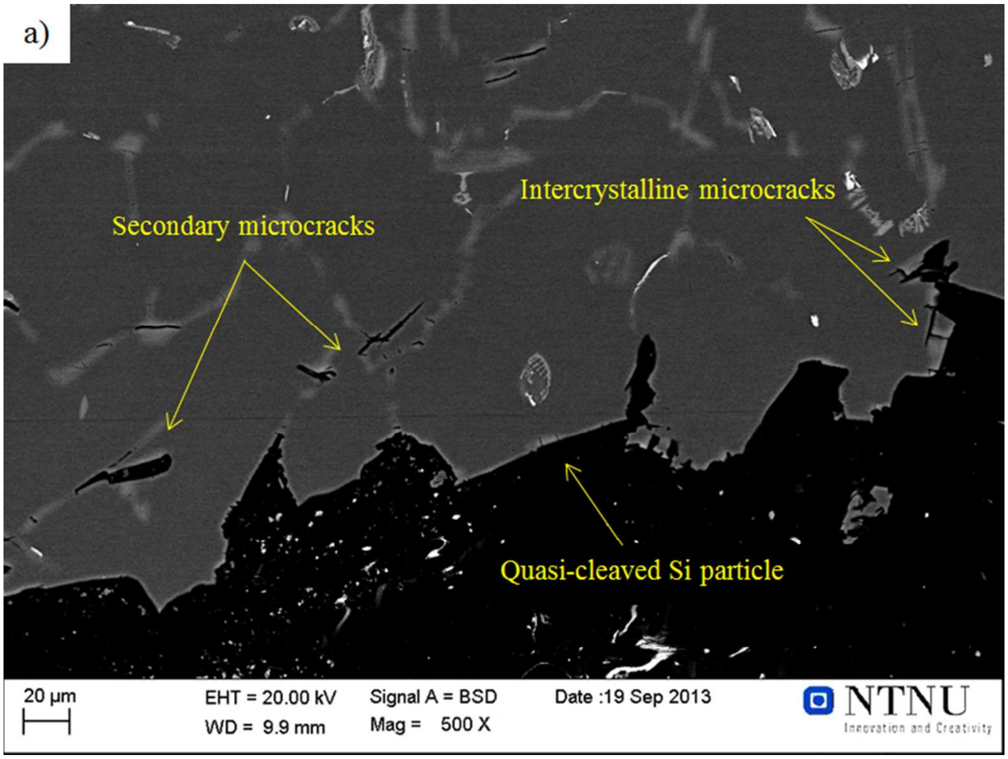

Fig. 10 BSE images of the fracture profile of the A356 reference alloy showing the Si-driven nature of impact fracture: a) sand mould, as-cast; b) sand mould, T6; c) permanent mould, as-cast; d) permanent mould, T6. Smaller SDAS are observed in permanent mould cast alloys implying the occurrence of local intergranular fracture c).
66x50mm (300 x 300 DPI)

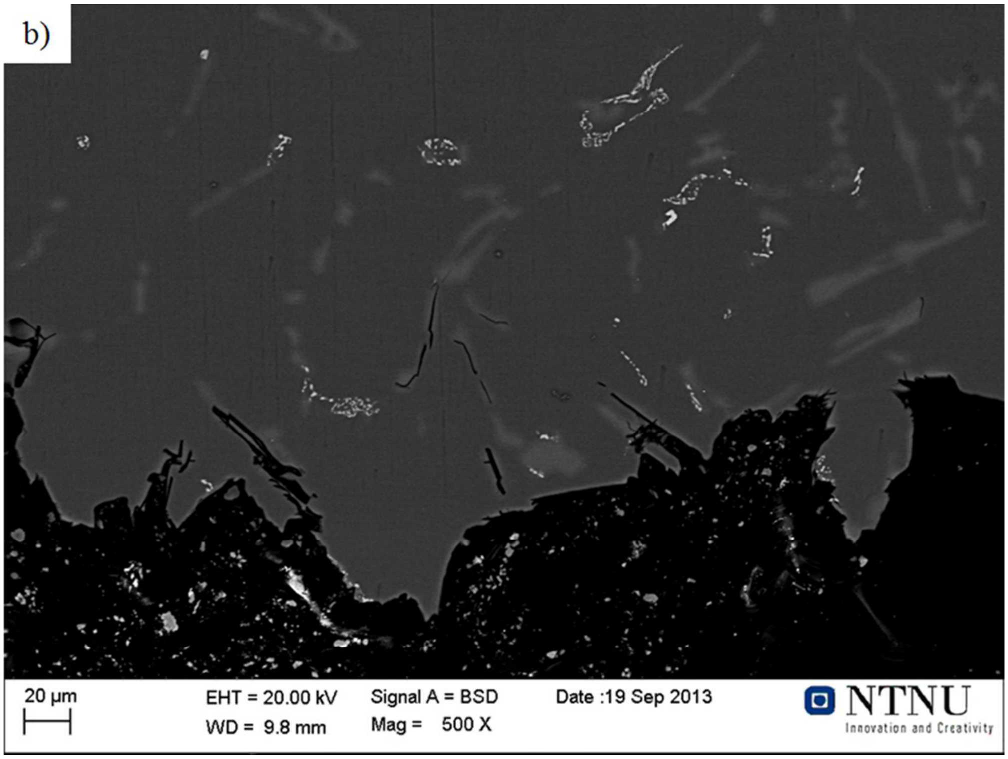

Fig. 10 BSE images of the fracture profile of the A356 reference alloy showing the Si-driven nature of impact fracture: a) sand mould, as-cast; b) sand mould, T6; c) permanent mould, as-cast; d) permanent mould, T6. Smaller SDAS are observed in permanent mould cast alloys implying the occurrence of local intergranular fracture c).
66x50mm (300 x 300 DPI)

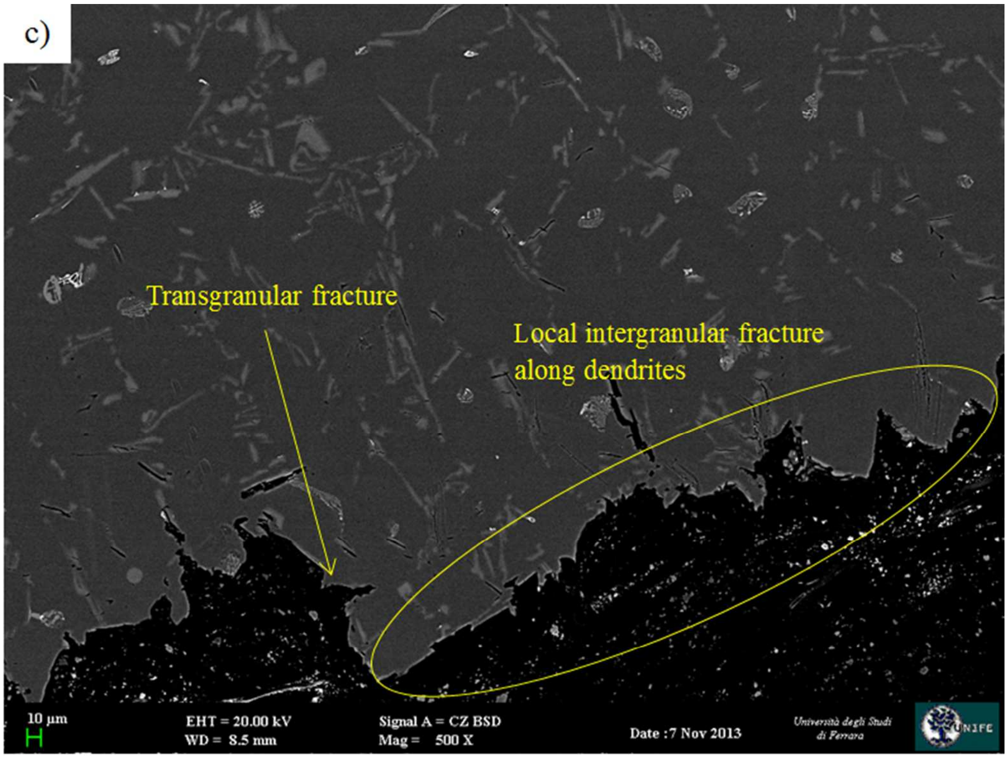

Fig. 10 BSE images of the fracture profile of the A356 reference alloy showing the Si-driven nature of impact fracture: a) sand mould, as-cast; b) sand mould, T6; c) permanent mould, as-cast; d) permanent mould, T6. Smaller SDAS are observed in permanent mould cast alloys implying the occurrence of local intergranular fracture c).
66x50mm (300 x 300 DPI)

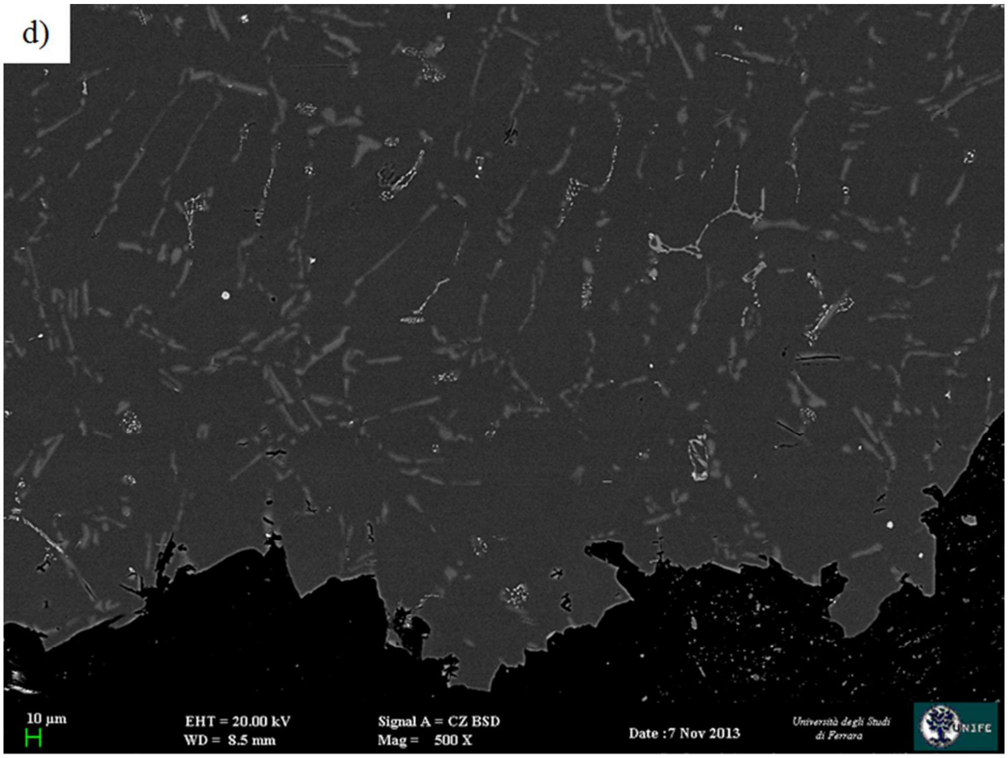

Fig. 10 BSE images of the fracture profile of the A356 reference alloy showing the Si-driven nature of impact fracture: a) sand mould, as-cast; b) sand mould, T6; c) permanent mould, as-cast; d) permanent mould, T6. Smaller SDAS are observed in permanent mould cast alloys implying the occurrence of local intergranular fracture c).
66x50mm (300 x 300 DPI)

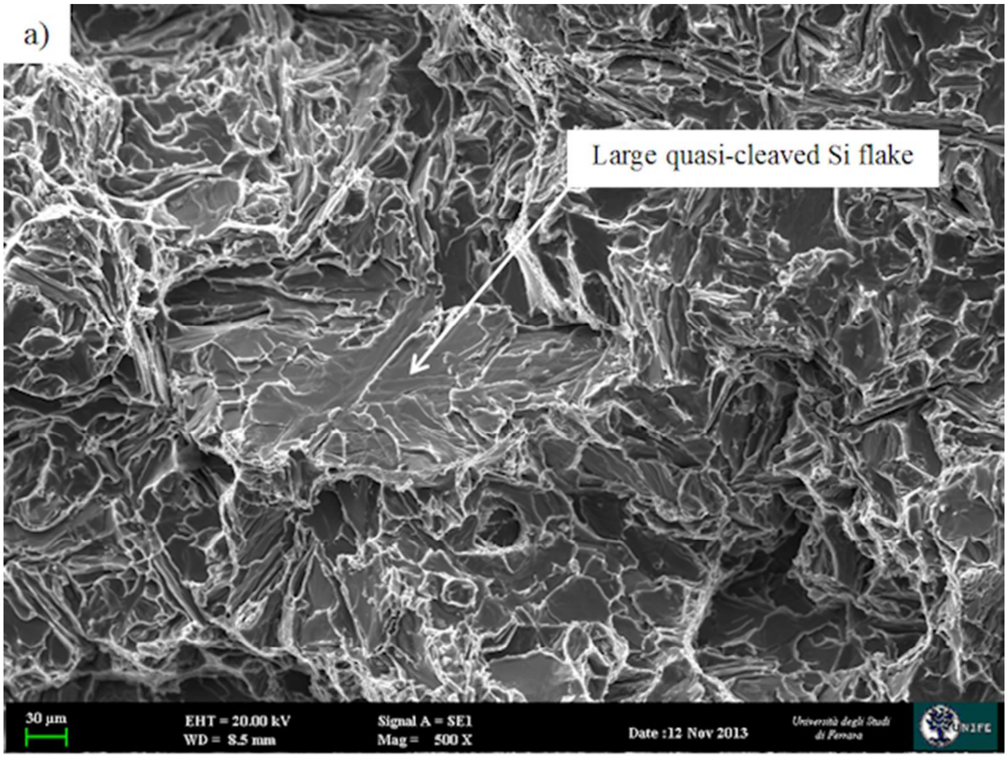

Fig. 11 SEM images of fracture surfaces of the A356 reference alloy showing the Si-driven nature of impact fracture: a) sand mould, as-cast; b) sand mould, T6; c) permanent mould, as-cast; d) permanent mould, T6. Note that the typical characteristics of fragile fracture still remain even in alloys where the effect of solution heat treatment appears to be more pronounced d).
53x40mm (300 x 300 DPI)

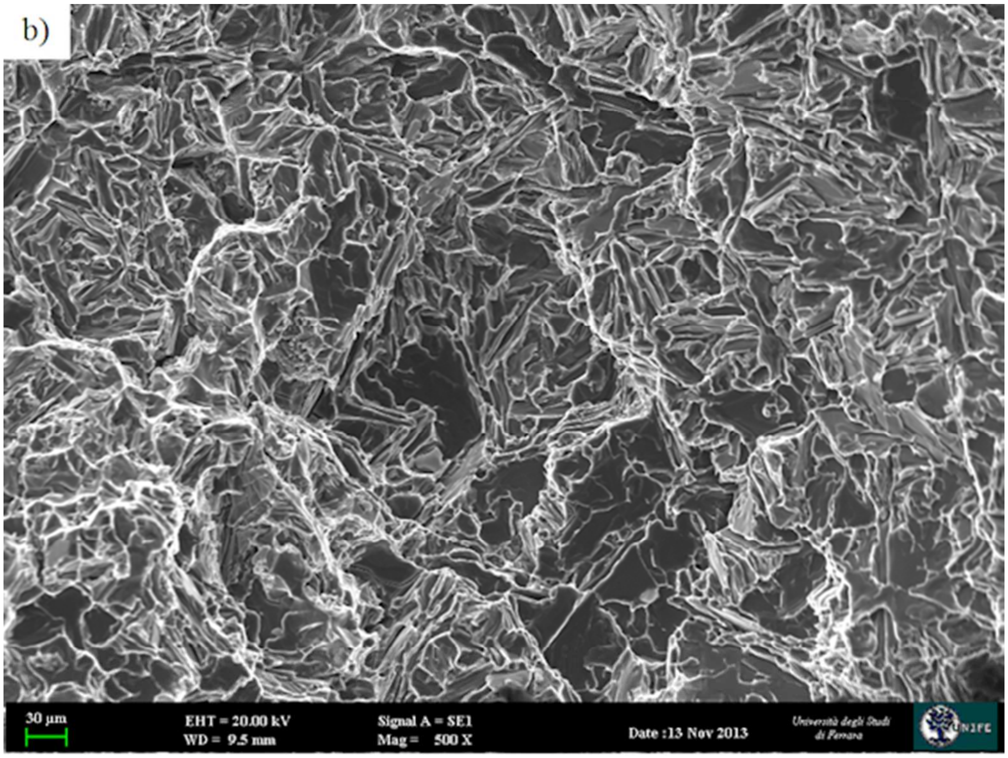

Fig. 11 SEM images of fracture surfaces of the A356 reference alloy showing the Si-driven nature of impact fracture: a) sand mould, as-cast; b) sand mould, T6; c) permanent mould, as-cast; d) permanent mould, T6. Note that the typical characteristics of fragile fracture still remain even in alloys where the effect of solution heat treatment appears to be more pronounced d).
53x40mm (300 x 300 DPI)

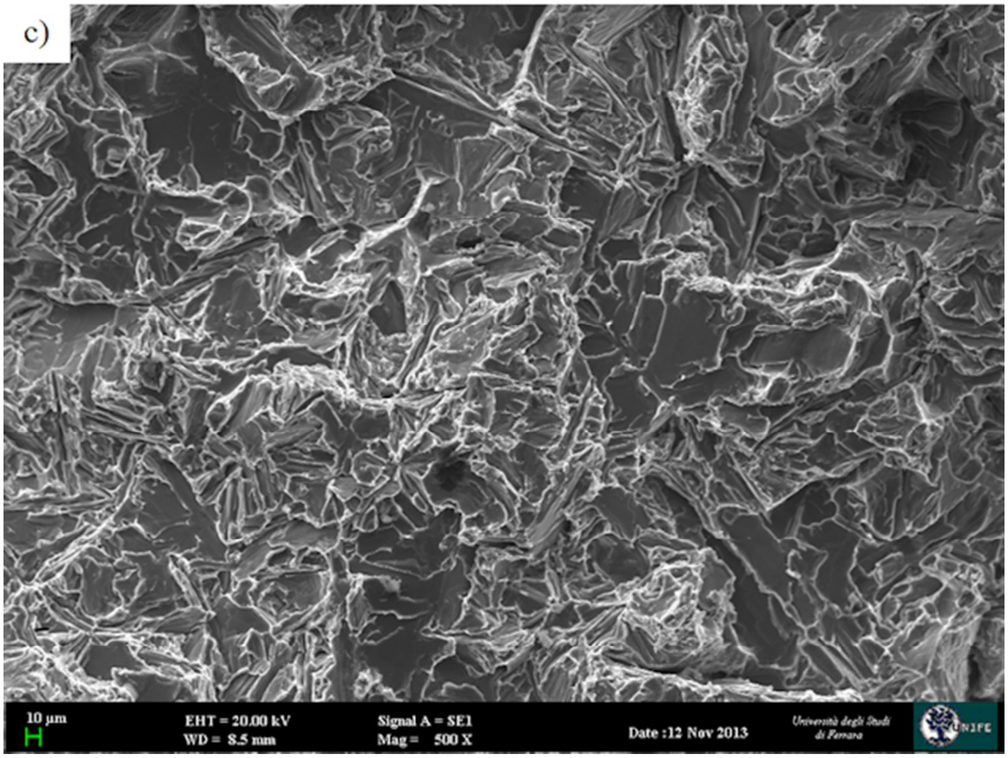

Fig. 11 SEM images of fracture surfaces of the A356 reference alloy showing the Si-driven nature of impact fracture: a) sand mould, as-cast; b) sand mould, T6; c) permanent mould, as-cast; d) permanent mould, T6. Note that the typical characteristics of fragile fracture still remain even in alloys where the effect of solution heat treatment appears to be more pronounced d).
167x125mm (96 x 96 DPI)

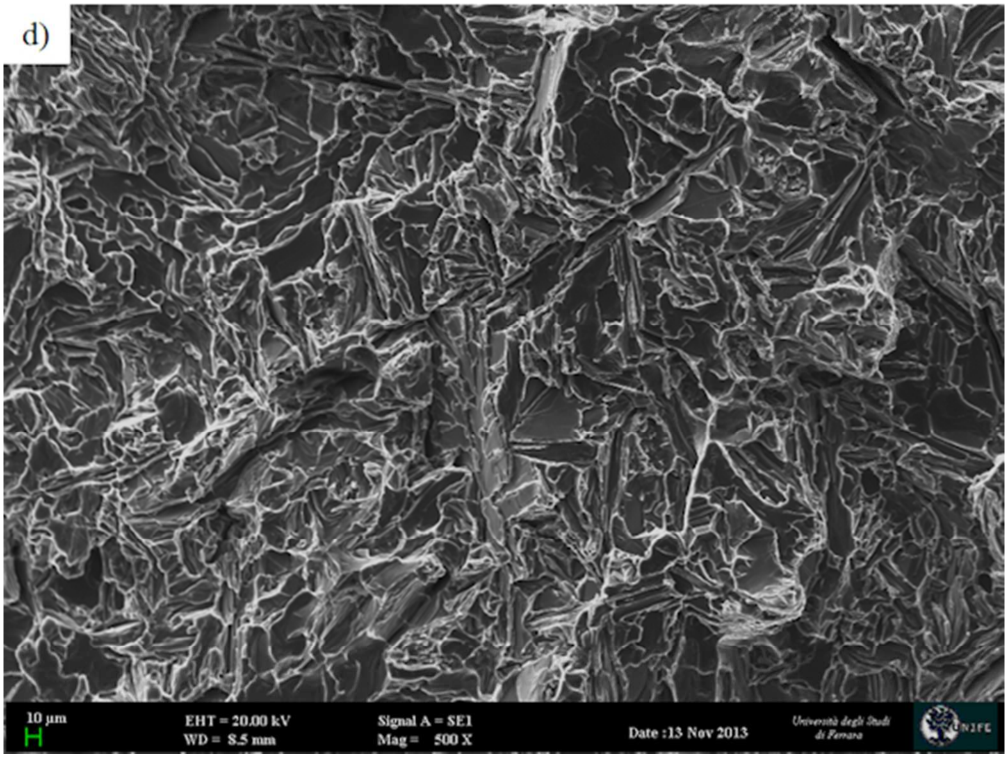

Fig. 11 SEM images of fracture surfaces of the A356 reference alloy showing the Si-driven nature of impact fracture: a) sand mould, as-cast; b) sand mould, T6; c) permanent mould, as-cast; d) permanent mould, T6. Note that the typical characteristics of fragile fracture still remain even in alloys where the effect of solution heat treatment appears to be more pronounced d).
53x40mm (300 x 300 DPI)